DYNAMICS OF SWASH AND IMPLICATION TO BEACH RESPONSE

Evans Waddell

Louisiana State University

Prepared for:

Office of Naval Research

March 1973

Coastal Studies Institute
Louisiana State University
Baton Rouge, Louisiana 70803

Technical Report No. 139

DYNAMICS OF SWASH AND IMPLICATION TO BEACH RESPONSE

By Evans Waddell

This research was supported by the Office of Naval Research through Contract N00014-69-A-0211-0003, under Project NR 388 002.

March 1973

61

R

Unclassified

Security Classification

DOCUMENT CONTROL DATA - R & D

Security classification of title, body of abstract and indexing annotation must be entered when the overall report is classified

1. ORIGINATING ACTIVITY (Corporate author)	2a. REPORT SECURITY CLASSIFICATION
Coastal Studies Institute Louisiana State University Baton Rouge, La. 70803	Unclassified
	2b. GROUP Unclassified

3. REPORT TITLE

DYNAMICS OF SWASH AND IMPLICATION TO BEACH RESPONSE

4. DESCRIPTIVE NOTES (Type of report and inclusive dates)

5. AUTHOR(S) (First name, middle initial, last name)

Evans Waddell

6. REPORT DATE	7a. TOTAL NO. OF PAGES	7b. NO. OF REFS
March, 1973	49	47

8a. CONTRACT OR GRANT NO	9a. ORIGINATOR'S REPORT NUMBER(S)
N00014-69-A-0211-0003 b. PROJECT NO NR 388 002 c d	Technical Report No. 139 9b. OTHER REPORT NO(S) (Any other numbers that may be assigned this report)

10. DISTRIBUTION STATEMENT

Approved for public release; distribution unlimited.

11. SUPPLEMENTARY NOTES	12. SPONSORING MILITARY ACTIVITY
	Geography Programs Office of Naval Research Arlington, Virginia 22217

13. ABSTRACT

A field investigation on a natural sand beach of the swash process and the interaction of swash with input waves, beach ground water, and beach sand levels was conducted on Santa Rosa Island, Florida. A high-resolution system of capacitance wire probes for field measurement of swash processes was developed. From field studies of swash phenomena it was found that the collision between uprush and backwash plays an important role in reducing the extent of swash runup and in partially filtering the effects of variations in the intensity of input waves. Water percolation into the beach matrix serves as a low-pass filter affecting swash frequency. Detailed sand-level observations indicate the presence of low-amplitude bedforms which migrated consistently downslope, suggesting that uprush sediment transport was primarily through suspension. (U)

DD FORM 1 NOV 65 1473 (PAGE 1)

S/N 0101-807-6811

Unclassified

Security Classification

A-31408

14 KEY WORDS	LINK A		LINK B		LINK C	
	ROLE	WT	ROLE	WT	ROLE	WT
Swash process						
Wave energy						
Tides						
Currents						
Beach processes						
Beach probe instrumentation						

Coastal Studies Institute
Louisiana State University
Baton Rouge, Louisiana 70803

Technical Report No. 139

DYNAMICS OF SWASH AND IMPLICATION TO BEACH RESPONSE

By Evans Waddell

March 1973

ABSTRACT

A field investigation on a natural sand beach of the swash process and the interaction of swash with input waves, beach ground water, and beach sand levels was conducted on Santa Rosa Island, Florida.

High-resolution analog measurements of these interaction parameters were made by using a specially developed sensor system consisting of resistance-wire and capacitance wire probes. An array of up to eight probes, aligned perpendicular to the local shoreline, produced several sets of synchronized multiple time series which were analyzed from stochastic as well as analytic approaches.

During uprush and the initial part of backwash, the leading edge of the uprush behaved in a manner similar to that of a unit mass released upward on a frictionless slope with an initial momentum and acted on only by the downslope component of gravity. It was found that the initial momentum at the base of the slope was higher than expected from characteristics of input waves. Inundation periods under the swash predicted by the nonlinear wave theory of Shen and Meyer (1962) agreed with the data within 30 percent. However, whereas the theory predicted only a single water depth maximum associated with the uprush, the data exhibited two water depth maxima within a single swash cycle: one associated with uprush and another with backwash. The second maximum, which occurred only on the lower beach, resulted from either (1) a retrogressive bore growing in height while moving seaward or (2) collision between backwash and the uprush from a succeeding swash. The phenomenon of collision was characteristic of real swashes and was a direct result of periodic input waves. The collision process was ignored in the mathematical theory of Shen and Meyer, which was based on consideration of a solitary input wave.

Swash power spectra consistently displayed three prominent peaks: (1) a high-frequency peak ($\sim$0.3 hertz), associated with the collision process, (2) an interswash peak at frequencies ($\sim$0.11 hertz) distinctly lower than the input wave frequencies, and (3) a beat frequency peak which appeared to be caused by standing waves in the nearshore. Increased input wave energy contributed significantly to intensification of collision process at the lower beach, such that (1) the high-frequency peak gained in height, (2) the interswash peak expanded toward low frequency with little change in height, and (3) the beat peak remained unchanged.

The beach ground water level exhibited fluctuations of both interswash and beat frequencies. The data indicated that the pressure head of the swash arriving at the shoreline induced an instantaneous response in a well 5 meters inland, followed by a lagged rise in water level. This lag resulted from the frictional retardation of horizonal mass flux traveling through a saturated beach layer. Thus, the beach matrix and beach slope both acted as a low-pass filter whose cutoff frequency underwent red shift with distance landward from the shoreline.

Sand level data revealed the possible presence of low-amplitude sand waves which persistently migrated downslope during both erosion and nonerosion. These

sand waves exhibited an average celerity on the order of 3-10 cm/sec and a -2 power frequency dependence below the equilibrium subrange.

ACKNOWLEDGMENTS

Financial support for this study was furnished by Coastal Studies Institute, Louisiana State University, under Contract N00014-69-A-0211-0003, Project No. NR 388 002, with Geography Programs of the Office of Naval Research.

The writer is indebted to Dr. C. J. Sonu for valuable advice and fruitful discussion during the course of this research program. Dr. Sonu's extensive critical review of this manuscript is greatly appreciated. Additional review by Drs. W. G. McIntire, S. A. Hsu, L. D. Wright, J. N. Suhayda, and J. M. Coleman was also very helpful.

Special thanks is extended to R. G. Fredericks for his work in development and construction of the capacitance probe measurement system, which was fundamental to this investigation. The able assistance of N. Rector, B. Montgomery, and M. Hernandez-Avila in instrument fabrication and field work is gratefully acknowledged.

Permission to use the beaches on the Air Proving Grounds, Eglin AFB, is appreciated. Thanks are extended to M. Cartledge for his help in arranging this permission.

CONTENTS

FIGURES

PHOTOGRAPHS

LIST OF SYMBOLS

A	amplifier, area, constant of proportionality
A_i	peak of input wave spectra
B	bicoherence of frequencies of f_1 and f_2
B_i	peak of swash spectra
C_{xy}	cospectra
C	capacitance, celerity
C_i	peak in ground water spectra
D	diodes, differential operator
d	distance between plates
f	frequency
g	gravity
GW	ground water well
h	water depth
h_o	undisturbed water depth
H	bore height
H_{xy}	transfer function
k	wave number
n	number
P_x	power spectral density function of x
P_{xy}	cross-spectral density function
Q_{xy}	quadrature spectral density function
Q_i	transistor
R_x	autocorrelation function of x(t)
R	resistor
S_o	input wave sensor
SP	swash probes

S_{nn}	Fourier Transform
t	time
T	total record length
T_i	transformer
u_o	initial velocity of swash
u	horizontal component of velocity
x	horizontal coordinate, Fourier Transform
$x(t)$	time series
$x_s(t)$	location of the leading edge of the swash mass
$y(t)$	time series
β	subaerial beach slope
γ	deceleration factor (= g tan β)
γ_{xy}^2	coherence function
η	sand level elevation
η'	dn/dx
σ	radial frequency
σ^2	variance
τ	lag
ϕ	angle of repose of sand, phase angle, subaqueous slope

INTRODUCTION

The subaerial beach is a dynamic environment characterized by complex interactions among a number of physical parameters. The scale, magnitude, and nature of these interactions govern the response of the beach system. This investigation has as its objective the disclosure of the input-response relationships among input waves, swash, beach ground water, and beach configuration. The principal interest in this study is centered on (1) swash dynamics, (2) interactions between input waves, swash, and ground water, and (3) the dynamic response of the beach surface to these processes.

Individual swashes produced by the breaking of waves at the shoreline have two major features: (1) uprush and (2) backwash. Uprush, which immediately follows the final breaking of a wave, is characterized by the upslope transport of a mass of water. At maximum run-up the leading edge of the water mass has zero velocity. Backwash is the downslope movement of the swash mass which follows maximum run-up. In many cases backwash collides with the uprush of a subsequent swash mass.

That portion of the beach slope which is directly in contact with the swash mass at any time during its cycle is here defined as the swash slope. The width of this region of contact varies in response to changing water levels, wave conditions, and across-beach profiles. It is generally limited landward by the maximum limit of uprush and seaward by the step.

The water table in the beach is a dynamic boundary which responds to inland ground water and to mass flux across the beach face. The water table intersects the beach face, and conditions of the beach surface differ greatly above and below the resulting line of intersection. Anything which causes this line to change position results in expansion and contraction of differentiated zones on the beach face.

Despite the large number of investigationsof swash and related processes, the physical mechanism of swash is not fully understood. Analytic description of swash requires a closed-form solution of nonlinear long-wave equations in the vicinity of the breakpoint. Presently, no theories exist which can provide this. The additional requirement of periodic input waves further complicates the solution.

Previous examinations of the dynamic beach system have generally lacked detailed measurements of related high-frequency processes. The highest rate of sampling of the beach configuration ever reported was at half-hour intervals (Strahler, 1966), and the highest sampling rate of beach ground water was at 10- to 15-minute intervals (Harrison et al., 1971). High-speed photography of swash has been used to permit continuous monitoring of the location of the leading edge of the swash mass (Emery and Gale, 1951), but it does not allow resolution of swash depth.

These technical difficulties were essentially solved by the measurement system developed by the Coastal Studies Institute, Louisiana State University, and used during this study. This system permitted simultaneous continuous measurements of (1) input wave characteristics, (2) swash configuration and characteristics, (3) sand level fluctuations on the swash slope, and (4) fluctuations of the water table in the beach matrix. It consisted of an array of as many as eight sensors located on a line perpendicular to the local shoreline. In general, a standard combination of seven probes was used: (1) a tsunami sensor and a wave sensor, both located seaward of the final breakpoint, (2) four swash probes on the active swash slope, and (3) a ground water probe behind the active beach face. On several occasions a second ground water probe was added to the array.

Water level fluctuations associated with incident waves prior to breaking at the shoreline were measured by a resistance-type wave probe, and the tsunami sensor measured beat fluctuations at the same location. Capacitance swash probes monitored local water depths on the swash slope during pa sage of a swash mass. These also monitored local wetted sand levels during the interswash periods. Capacitance ground water probes had identical detector circuits which could be interchanged from one configuration to the other.

The sensors produced continuous analog signals which were recorded as simultaneous time series on multichannel strip charts. These data could be readily subjected to stochastic analysis after digitization at an appropriate sampl ng interval. Time-synchronized swash records at several stations on the beach slope also allowed for construction of a history of across-beach configuration which could be compared with that predicted by existing mathematical models.

LITERATURE

Swash dynamics and associated processes have been studied extensively. Existing literature can be divided into three major categories in accordance with differing goals or approaches: (1) engineering studies on run-up, (2) analytical studies, and (3) field studies which included beach ground water as one documented parameter.

ENGINEERING STUDIES

Reliable estimation of run-up is important in designing coastal structures such as dikes and breakwaters. Consequently, engineering studies have dealt almost exclusively with investigations of this aspect of swash. These studies have attempted to reveal the degree of dependence of run-up on such parameters as (1) slope of the structure, (2) wave heights, periods, and angles of incidence (Hosoi and Mitsui, 1963; Saville, 1957), (3) differing breakpoints relative to the base of the slope (Granthem, 1953), and (4) whether input waves are solitary (Hall and Watts, 1953; Kaplan, 1955) or periodic (Van Dorn, 1967). The influence of characteristics of the slope surface such as permeability (Savage, 1959) and hydraulic roughness (Hudson, 1959) was also investigated.

The engineering approach progressed from initial considerations of solitary waves and monochromatic wave trains to more recent consideration of dissimilar or random wave trains. Van Dorn (1967) investigated the differing characteristics of run-up produced by a train of monochromatic waves as opposed to that from a solitary wave of the same height. Other investigators used wind tunnels to approximate more realistically run-up of "natural" wind waves (Sibul and Tickner, 1956). Generally, the empirical approach was not successful but did emphasize that the natural run-up phenomena could not be treated as a strictly deterministic process.

Several recent studies have considered run-up as a stochastic process with a particular distribution function (Saville, 1963). The random component in the swash process results from such things as (1) randomness in input wave characteristics (Collins and Wier, 1969), (2) varying patterns of interference between uprush and backwash, and (3) time-dependent environmental parameters such as level of the water table, sand texture and size distribution, and nearshore topography.

One study which considered run-up as stochastic is by Battjes (1971), who, using an equivalence assumption, determined an expression for the run-up distribution. This distribution was a function of wave height and period and of beach slope. Differing sea states, as indexed by the correlation between offshore wave height and period, could be taken into account. Even though formulation of maximum run-up height was based on the empirical relation of Hunt (1959), testing of the distribution against field data taken on a cement breakwater indicated good agreement with the hypothesized Rayleigh distribution.

These engineering studies were generally concerned with empirical relations and not with physical mechanisms of swash. The empirical data exhibited such extensive scatter that it precluded establishment of specific functional relations

from them.

ANALYTICAL STUDIES

LeMéhauté (1963) and associated investigators (LeMéhauté et al., 1968) studied run-up by means of nonsaturated breaker theory. The assumption was made that a solitary input wave moving over a sloping bottom is capable of sustaining a certain maximum energy density and a certain maximum onshore energy flux. By balancing changes in energy associated with the wave form with changes in onshore energy flux, it was possible to derive a criterion to determine whether a given wave will be (1) nonbreaking, i.e., nonsaturated, (2) spilling, or (3) a fully developed bore, i.e., saturated.

Critical parameters controlling this criterion are (1) beach slope and (2) bottom friction coefficient. These are related in such a way that, for a given wave, the greater the friction coefficient, that is, the greater the frictional dissipation of energy, the steeper the slope which will sustain a nonbreaking, nonsaturated wave. A nonsaturated wave produces no swash because all energy is dissipated before the wave form reaches the shoreline.

Because of limitations on the value of the friction coefficient, there is a slope value which if exceeded will always produce a fully developed bore, regardless of the initial wave. The implication is that, for all slopes greater than this value, solutions converge to similar forms. This relation gives rise to the concept of "forgetfulness" of input waves; that is, behavior of waves becomes independent of prior history. The critical slope value appears to be 1 percent if it is assumed that the friction coefficient is 0.01 or less. Further study has indicated that this friction coefficient may be too small. Thus the critical slope would be greater than 1:100.

Historically, the difficulty in pursuing a rigorous mathematical treatment of swash has been that incident waves approaching the shoreline are essentially nonlinear. Stoker (1947) was among the first to solve nonlinear long wave equations by the method of characteristics and to explain formation of breakers and bores on a sloping seabed. Biesel (1951) arrived at similar results by dealing with the problem in a Lagrangian coordinate system. Extension of these processes onto a beach slope to explain swash phenomena was first accomplished by Shen and Meyer (1962).

In their treatment, a mathematical singularity arises as the bore arrives at mean sea level - swash slope intersection, which is the initial shoreline. The incoming bore collapses at this point, where two characteristic lines, one representing the bore front and the other the shoreline, merge. Shoreward of this point, the leading edge of the swash is treated as the time-dependent displacement of the shoreline.

Three major conclusions of these studies were as follows: (1) velocity of the leading edge tends to a finite positive value at the base of the beach slope, (2) deceleration of the leading edge is constant, and (3) deceleration is a direct function of the beach slope. In the vicinity of the limiting characteristic, which defines the path of the leading edge in a time-space domain, water depth was found to be proportional to the square of the distance from the shoreline. Also, at some small distance behind the moving shoreline, i.e., the leading edge, the water depth is proportional to the -2 power of the travel time after bore collapse.

During the latter part of backwash, an additional characteristic occurs in the solution. According to Shen and Meyer, this characteristic indicates formation of a retrogressive bore; that is, a bore which faces upslope while migrating downslope. When this bore develops, conditions on the previous characteristics are no longer appropriate.

In a laboratory study Miller (1968) checked some predictions of this theory and found that (1) run-up height relative to bore height was not accurately predicted by long wave theory and (2) only partial collapse of the bore front occurs as the bore encounters the subaerial beach slope. Miller felt that consideration of friction would improve results and the agreement.

Meyer (1970) compared analytical theory against experiment and found that the basic mechanism identified in long wave theory is correct, although some discrepancies in magnitudes of real and predicted variables occurred. Meyer suggested that inclusion of dissipative forces would greatly increase agreement inasmuch as energy dissipation is a significant factor on the beach face.

The Shen and Meyer approach involved the following assumptions and associated shortcomings: (1) each wave completed an entire swash cycle prior to arrival of another wave at the initial shoreline, i.e., there was no collision between successive swashes, (2) each wave had the form of a bore prior to arrival at the initial shoreline, i.e., input wave was similar to a breaker, (3) mass on the swash slope was conserved, i.e., there was no loss as a result of seepage, and (4) the swash slope was constant, i.e., there was no response of beach topography. Their approach did not supply closed-form solutions to this simplified situation.

FIELD STUDIES

From detailed visual and photographic observations Emery and Gale (1951) were able to infer interrelationships between incident waves, swash, and ground water. They described (1) small changes in beach ground water induced by individual swashes and (2) evolution of across-beach profiles of swash during its cycle. It was noted that swash moved up the beach as a mass with a small steep-faced front and that it retreated seaward in such a way that the swash thinned without significant change in location of the leading edge until most of the water had moved down the beach face.

One of the most important points of their observations was that smaller high-frequency breakers disappeared prior to moving up the beach as swash. Because of this, they suggested that the beach acts as a filter which permits passage of only larger or longer waves. They also observed that the period of swash was always larger than that of input waves seaward of the shoreline. They noted that the gentler the slope, the greater the difference between the periods of swashes and input waves. This they attributed to interaction of successive swash masses.

Also mentioned in Emery and Gale's study were beat fluctuations of offshore water level, which they associated with sequential arrivals of groups of low and high waves (see also Tucker, 1950).

Specific attempts to establish effects of ground water on beach changes were made by several investigators, among them Emery and Foster (1948), Grant (1948), Longuet-Higgins and Parkin (1962), Duncan (1964), and Pollack and Hummon (1971). Emery and Foster (1948) found that during ebbing tide the water table near the beach face sloped seaward, whereas during flooding tide the water table sloped landward. They indicated that response of the beach ground water to tide was

inversely proportional to distance from the beach face. They reasoned that "vertical permeability [of the beach] must be lower than horizontal permeability because beaches contain thin alternating coarser and finer layers" (p. 648). Horizontal mass flux was associated with movement of the tidal wave through the beach matrix behind the swash slope.

Grant (1948) recognized that height of the ground water table was related to whether the beach was prograding or eroding. The model which Grant presents for this relation indicates that a dry beach facilitates deposition on the foreshore by reducing backwash flow velocity and thus prolonging existence of laminar flow. On a saturated beach, backwash is supplemented by outflow through the zone of effluent which makes backwash turbulent earlier in the cycle. Outflow also dilates sand grains in this region, which further encourages erosion.

Longuet-Higgins and Parkin (1962) found that when an impermeable roofing-felt was inserted in the beach about 3 inches below the sand surface "the waves quickly eroded the shingle overlying the roofing-felt but disturbed only to a lesser extent the shingle on either side" (p. 196). These investigators attributed these results "to the fact that over the roofing-felt, the backwash could not penetrate to a depth of more than three inches, and so, the backwash there was relatively undiminished."

Duncan (1964) investigated combined influences of semidiurnal tidal and ground water fluctuations on deposition and erosion in the swash zone. During flooding tide, sand that was deposited on the beach slope above the water table was taken from the region below the water table. This deposition was associated with loss of swash mass as a result of infiltration and consequent decrease in seaward acting momentum. As infiltration continued, the ground water table elevated, thus causing the lower boundary of the zone of infiltration to migrate landward. There was also evidence of an associated outflow lower on the beach face. This outflow dilated sand grains to encourage further erosion on that portion of the slope. On the other hand, during falling tide part of the zone of infiltration was removed from swash influence, and consequently little mass was lost to infiltration. Backwash was, in fact, enhanced by outflow of ground water, which caused a pad of material to move downslope until the profile approximated the initial low-tide configuration.

Pollack and Hummon (1971) identified four beach zones on the basis of both degree of saturation and spatial and temporal changes of water content. In order of occurrence down the beach face, the zones are (1) dry sand, (2) retention, (3) resurgence, and (4) saturation.

The zone of dry sand was influenced by swash action only during occasional tidal cycles. The zone of retention was influenced by swash for some period during all tides; therefore, sand in this region was never completely dry. During time of exposure, water content was controlled by gravity. This zone was porous and involved a great deal of inflow and outflow. The zone of resurgence was characterized by intensive mass flux throughout the tidal cycle. This zone expands and contracts depending on the amount of circulation and the discrepancy between nearshore water level and the water table of the beach. The zone of saturation remained saturated under all conditions of tide and swash.

Common to these field studies are two critical shortcomings: (1) the data were collected neither at sufficiently high resolution nor at sufficiently high frequency to provide insight into the actual physical mechanisms, and (2) because the pertinent first-order parameters were not measured simultaneously the real-time

interaction between input waves, swash, ground water, and beach change could not be established. Furthermore, results from these studies were mostly qualitative. Most of these shortcomings were overcome by the measurement system employed in the present investigation.

METHODOLOGY

SITE DESCRIPTION

This field experiment was conducted between June 27 and July 3, 1971, on Santa Rosa Island, Florida, a barrier island on the northwest coast of Florida. This investigation of swash was one aspect of the multidisciplinary SALIS (Sea-Air-Land Interaction System) study of a nearshore open coastal environment. The multidisciplinary character of SALIS produced a broad-based integrated data set which was available to each component project. Consequently, a coherent documentation of all parameters pertinent to each project was available. For studying beach dynamics, supporting data regarding wave climate, meteorological conditions, and tide level were supplied. The beach dynamics project, of which swash dynamics is one component, additionally involved continuous documentation of the behavior of beach ground water at five different across-beach locations. These data are not included in this discussion.

During the study period, the beach consisted of a berm about 50 feet wide plus an active beach about 15 feet in width. The beach was composed of very well sorted medium sand; mean size was in the range of 250-300 microns. Composition of the sand was 95 percent pure quartz, and there was very little shell content (see Photographs 1 and 2).

The slope of the active beach was comparatively steep, in many cases being greater than 1:10. A rhythmic topography (Hom-ma and Sonu, 1962; Sonu, 1973) with a wavelength on the order of 200 meters existed in differing stages of development.

Wave conditions during the investigation were dominated generally by swells from the southwest. Local wind waves generated by a diurnal sea- and land-breeze cycle were superimposed on this basic wave field. The peak component of the wind-wave spectra appeared at approximately 9:30 a.m. and increased toward evening while rotating in a clockwise direction and shifting the peak frequency toward the lower frequency side. Local wind waves degenerated between evening and the following morning as the sea breeze was replaced by the land breeze.

Tide was diurnal, having tropic and equatorial phases recurring approximately every 14 days. Maximum tidal range during the study (see Fig. 2) was approximately 15 cm.

Ground water in the beach sand was distinctly cooler than the seawater, and, depending on location of measurements, amount of mixing, rainfall, etc., less saline than seawater. No rainfall occurred during the study period. Salinity distributions were not investigated.

A number of experimental runs were conducted with a variety of sensor combinations. Of these, data resulting from combinations of one or two ground water probes, four swash probes, one input wave probe, and one tsunami probe were most intensively analyzed inasmuch as they represented interactions among principal parameters (Fig. 1). These data are based on Runs #1, #3, #5, and #6, of which Run #1 used two ground water probes, whereas during other runs only one ground water probe was used. Each experimental run lasted 2 hours, although, for this

Photograph 1. General scene of the site. Note arrays of swash probes and ground water wells near an apex of the rhythmic shoreline and an instrument trailer in the backshore. A dark dye streak in the water shows a rip current. Poles in the foreground are cup anemometers used in a complementary study of the SALIS Project (Sea-Air-Land Interaction System), of which this study is a part.

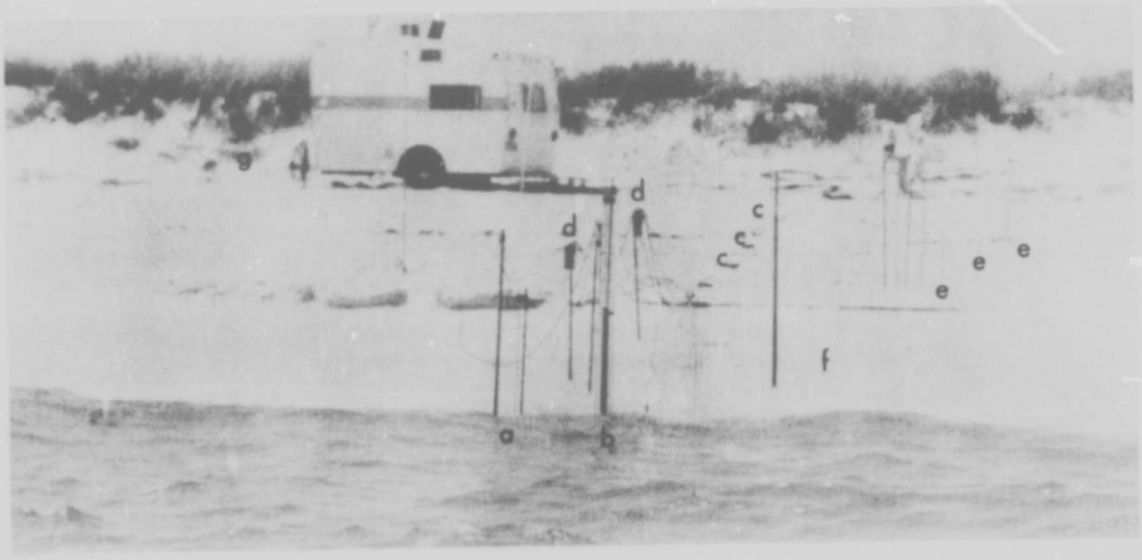

Photograph 2. Closeup view of the probe system. a. Wave gage; b. beat gage; c. swash probe; d. detector circuit package; e. ground water well; f. beach profile survey stakes; g. trailer housing electronics and recorder system.

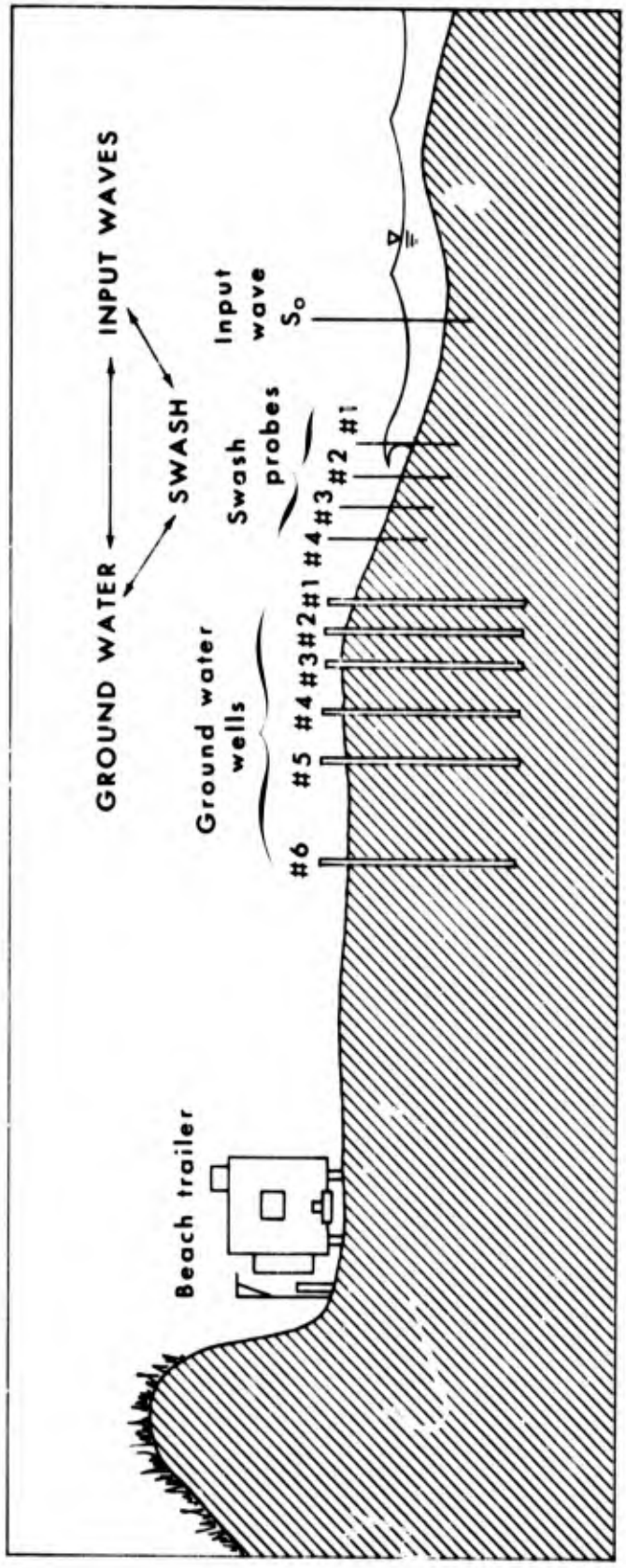

Figure 1. General beach section and instrument location.

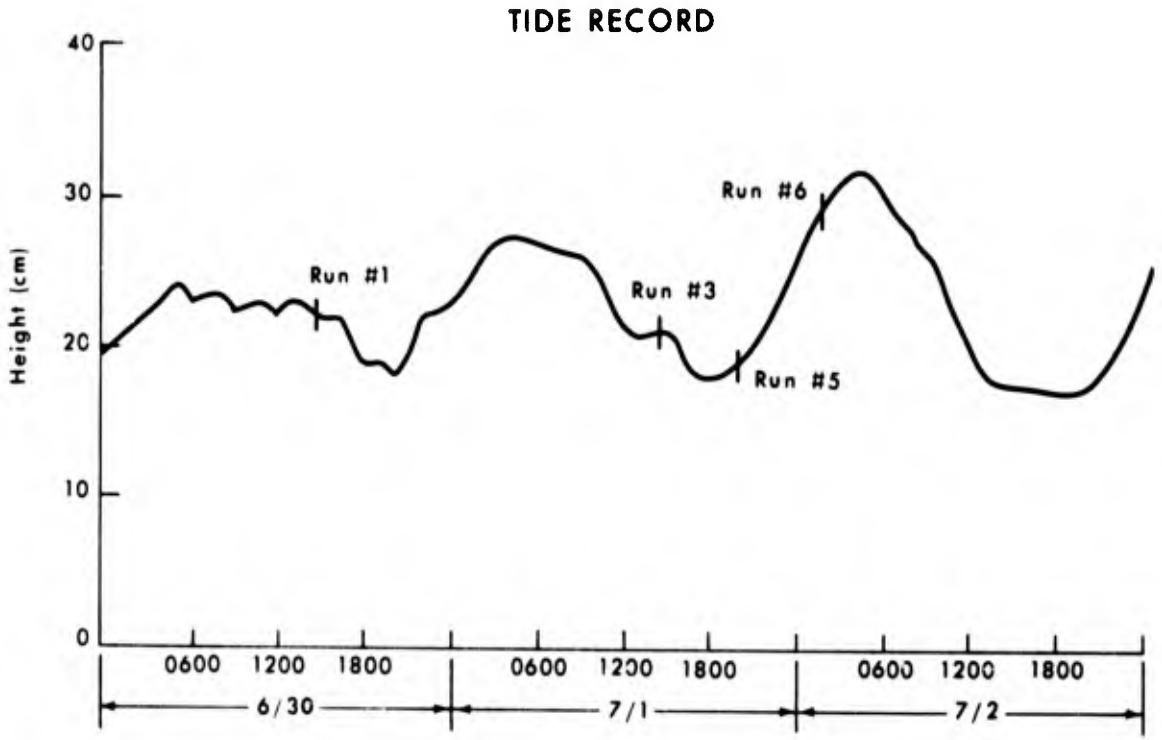

Figure 2. Tide record during the period of investigation. Beginning times for data runs are indicated on the curve.

study, only 15-minute records were used. Beginning times for each sampling period are indicated on Figure 2.

Probes were placed on a line across the beach perpendicular to the local shoreline. In plan view, this line was midway between a bay and horn of the rhythmic topography. About 5 meters seaward of the breakpoint was input wave sensor, S_O. On the active beach face were four swash probes, SP #1 - SP #4, spaced at 1-meter intervals up the beach. Two meters landward of the uppermost swash probe was the first ground water well, GW #1. One meter farther landward was the second ground water well, GW #2 (Fig. 1).

During Runs #1, #3, and #5, the mean breakpoint was just seaward of SP #1. Prior to Run #6, the location of the breakpoint had migrated landward and was approximately 30 cm seaward of SP #2. Consequently, SP #2 in Run #6 and SP #1 in Runs #1, #3, and #5 occupied the same location relative to the breakpoint.

INSTRUMENTATION

High-resolution and continuous measurement of variables was fundamental to this study. The measurement system which produced these data was developed by CSI technical staff.

Swash and ground water measurements were made with two configurations of a capacitance-type probe connected through identical signal-processing circuits to a multichannel recorder. Output of one configuration, the swash probe, is a time history of (1) water depth of the swash as it runs across the probe and (2) sand

level of the wetted beach surface between swash arrivals. Output of the other configuration, the ground water probe, is a time history of fluctuations of the beach water table. Placing a row of probes across the beach permits recording of spatial and temporal distributions of these phenomena over the entire beach profile as synchronized multiple time series.

Principal advantages of this system over more conventional resistance systems include (1) independence with respect to variations in salinity and temperature and (2) strictly linear response. The first advantage is of particular importance because salinity and temperature of ground water can change with time and differ from that of swash. Response of capacitance probes is linear along the entire length, whereas with a comparably sized single straight-wire resistance probe linearity cannot reasonably be obtained. A modified resistance system with a wire spirally wrapped around a threaded circular rod (Truxillo, 1970) overcomes many linearity problems. However, our experiments show that in high-velocity fields such as swash, even a one-half-inch-diameter rod generated a potential head on the upcurrent side, preventing accurate resolution of swash depths.

Probes

Schematics in Figure 3 show configurations of swash and ground water probes. The probe consists of a metal lead encased in a synthetic jacket. When immersed in water, one plate of the capacitor is the lead and the other plate is the water. The dielectric is provided by the jacket. The resulting capacitance, C, is given by

$$C = \frac{A}{d} \tag{1}$$

where A is the plate area and d is the distance between the plates; hence, for a given uniform dielectric thickness, capacitance is linearly proportional to the immersed length of the probe.

In order to eliminate formation of a potential head on the upstream side of the swash probe, a lead wire with sufficiently small diameter was chosen. Minimum thickness of this wire was dictated by the need to incorporate a certain amount of tension so that it would be able to withstand swash impact. The configuration adopted was a PVC-coated, 22-gage, solid-core copper wire stretched vertically between two supporting PVC blocks. These blocks were held by a pair of stainless-steel rods, one of which served as the water ground.

The lead of the ground water probe consisted of a stainless-steel rod (diameter 0.95 cm) inserted in a tight-fitting Plexiglas tube (0.95 cm ID, 1.3 cm OD). This was held by two circular PVC plugs supported by a stainless-steel tube (diameter 0.64 cm), which was the water ground. A tight fit between the rod and the Plexiglas tube, as well as uniformity in the thickness of the latter, is essential for maintaining a linear capacitive response. The lead was sealed at both ends with epoxy resin to make it watertight.

Circuit Description

Schematics in Figure 4 show the electronic circuit. The entire circuit consists of three subsystems: (1) precision voltage regulator, (2) detector, and (3) output signal control. The detector circuit is similar to the one developed by McGoldrick (1969).

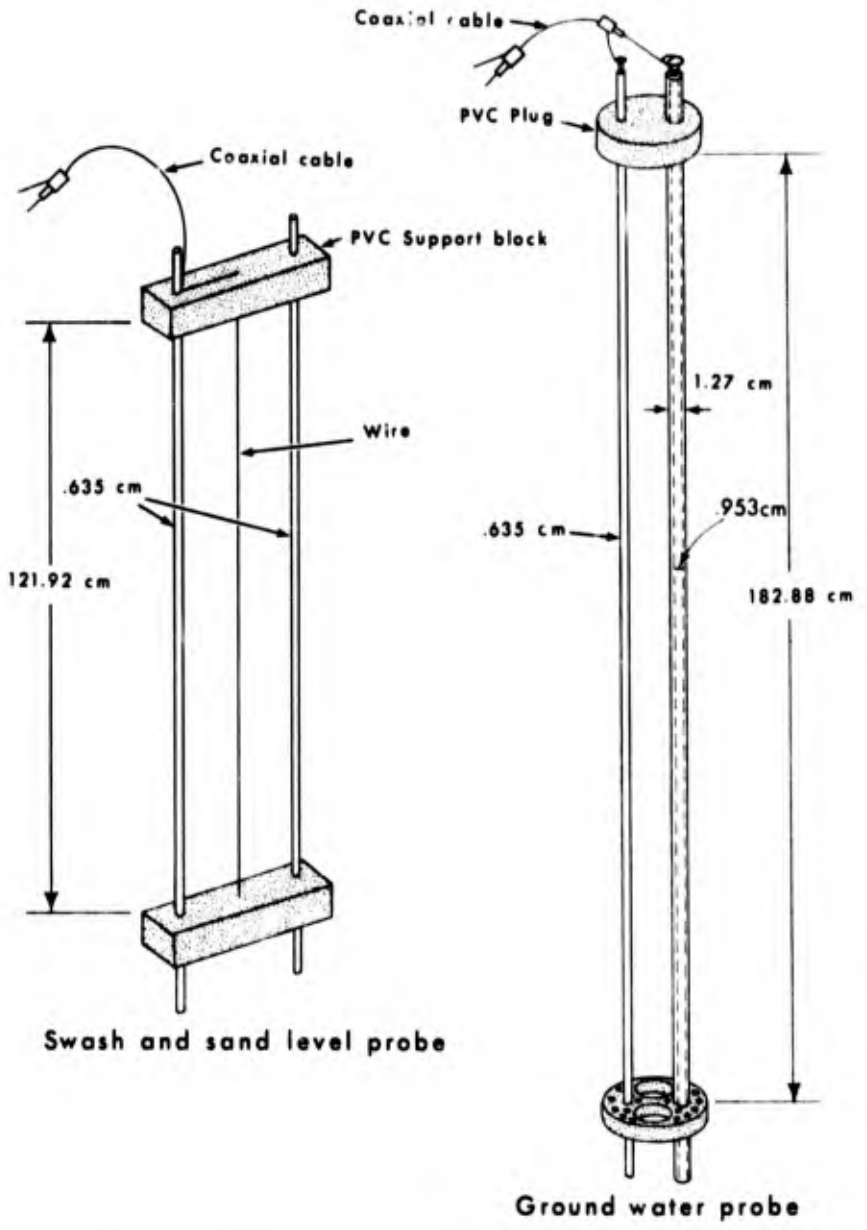

Figure 3. Schematics of both ground water probe and swash probe, indicating general configuration.

With the system operating, any voltage between 23 and 37 volts DC is applied to integrated circuit, U_1, in the precision voltage regulator, which results in a regulated 20-volt output. This output is split into two 10-volt sources by voltage dividers, R_5 and R_6. The center of this divider drives an operational amplifier, U_2, connected as a sources follower. The result is a balanced +10 and -10 volt output with common.

The +10 volt output is applied to the detector. The transistor, Q_1, in the detector, connected as a Hartly oscillator, generates a 455 kHz sinusoidal signal. This signal is inductively coupled by T_1 to a complementary transistor pair, Q_2 and

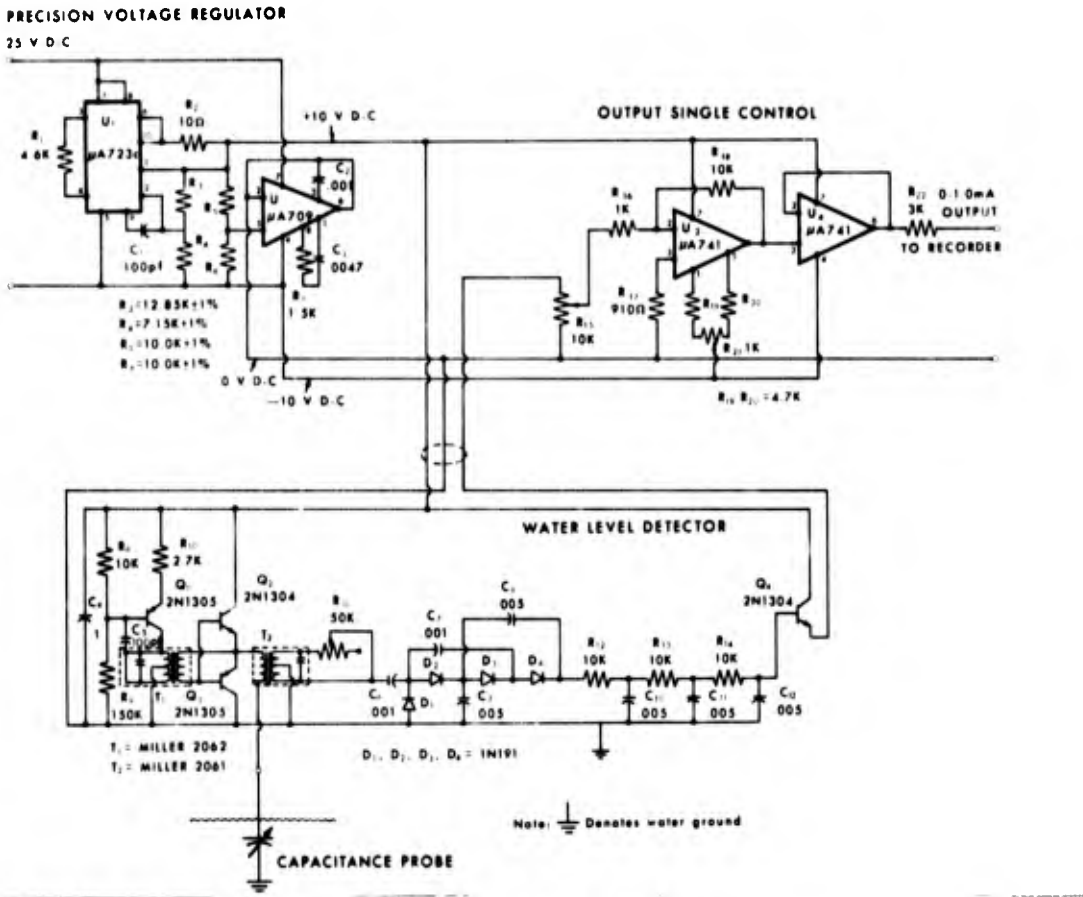

Figure 4. Circuit diagram for capacitance probes.

Q_3, which are biased between 0 and the +10 voltage supply. The resulting output is a 455 kHz square wave at constant 10 volt amplitude. This square wave is series-fed through the primary of the output transformer, T_2, to the capacitance probe.

A variation in capacitance caused by water level fluctuations on the probe results in a change in probe impedance. This change in turn alters the primary current of T_2 and, hence, its induced secondary voltage. This signal is an amplitude-modulated waveform varying with the water levels on the probe. The signal is then demodulated by diodes D_1, D_2, D_3, and D_4 and filtered by a three-stage R-C filter. The resulting DC output is amplified by Q_4 and sent to the output signal control.

The signal output from the detector is fed through potentiometer R_{15} to operational amplifier A_3. Here the signal is amplified and fed to U_4, a source-follower operational amplifier, which is used only to match the output signal level and is therefore useful as a "full-scale adjustment." Zero control is provided by R_{21}.

The precision voltage regulator and output signal control subsystems are housed in a single package located adjacent to the recorder. The detector subsystem, housed in a waterproof container, is placed adjacent to the probe. Because capacitance inherent to the connecting wire between the probe and detector subsystem can reduce sensitivity and linearity of the output signal from the probe, it is

essential to minimize the length of the connecting wire. According to our field test, a length up to about 50 cm can be tolerated.

Field Test

The system was tested in the field at Fort Walton, Florida, for 15 days in June 1971.

Swash probes were set vertically in the sand and their lower blocks buried about 10 cm below the sand level. During the field program repeated calibration checks showed that these probes, after an extended period of handling and use, could develop relaxation of wire tension, and readjustment of the probe tension and recalibration were required. In comparison, the ground water probe, although used extensively, maintained its original calibration during the entire experiment. This greater stability occurred as a result of the probe configuration.

DATA PROCESSING PROCEDURES AND TECHNIQUES

In view of the time series nature of the data, standard stochastic data analysis (Blackman and Tukey, 1958; Bendat and Piersol, 1966; Kisel, 1969) was performed. If x(t) is a randomly fluctuating stationary time series, then the autocorrelation function, $R_x(\tau)$, is defined as

$$R_x(\tau) = \lim_{T\to\infty} \frac{1}{T} \int_0^T x(t)\, x(t+\tau)\, dt \qquad (2)$$

where τ is the lag. $R_x(\tau)$ is an even function and has a maximum of 1 at $\tau = 0$. The Fourier Transform of the correlation function is the spectral density function, $P_x(f)$,

$$P_x(f) = 2 \int_0^\infty R_x(\tau)\, e^{(-j2\pi f\tau)}\, d\tau \qquad (3)$$

where f is frequency. For a zero mean process

$$P_x(f) = \sigma^2(f) \qquad (4)$$

and

$$\int_0^\infty P_x(f)\, df = \overline{x^2(t)} \qquad (5)$$

where $\overline{x^2}$ is the variance of the time history.

Given another randomly fluctuating stationary time series, y(t), the cross correlation function is given by

$$R_{xy}(\tau) = \lim_{T\to\infty} \frac{1}{T} \int_0^T x(t)\, y(t+\tau)\, dt \qquad (6)$$

and the Fourier Transform of this function is the complex cross-spectral density function

$$P_{xy}(f) = \int_{-\infty}^{\infty} R_{xy}(\tau)\, e^{(j2\pi f\tau)} d\tau \ . \tag{7}$$

This is a complex function which is given by

$$P_{xy}(f) = C_{xy}(f) + j\, Q_{xy}(f) \tag{8}$$

where $C_{xy}(f)$ is the coincident or cospectral component and $Q_{xy}(f)$ is the quadrature spectral component. These are also even and odd components, respectively, of the cross-spectral function.

In complex polar notation the cross-spectral density function is

$$P_{xy}(f) = |P_{xy}(f)|\, e^{j\phi_{xy}(f)} \tag{9}$$

where

$$P_{xy}(f) = (C_{xy}^{\ 2}(f) + Q_{xy}^{\ 2}(f))^{1/2} \tag{10}$$

and

$$\phi_{xy}(f) = \tan^{-1} (Q_{xy}(f)/C_{xy}(f)). \tag{11}$$

$\phi_{xy}(f)$ is the phase angle and indicates, as a function of frequency, phase relations between periodic components of x(t) and y(t).

The coherence function is defined as

$$\gamma_{xy}^{\ 2}(f) = \frac{P_{xy}(f)^2}{P_x(f)\, P_y(f)} \leq 1 \tag{12}$$

and is a normalized correlation function in frequency space.

In considering input-output relations of a linear system, two important relationships are

$$P_y(f) = |H_{xy}(f)|^2\, P_x(f) \tag{13}$$

and

$$P_{xy}(f) = H_{xy}(f)\, P_x(f). \tag{14}$$

$H_{xy}(f)$ is the systems function or frequency response function and describes amplitude attenuation between input and output as a function of frequency.

If the system is nonlinear, then the transfer function is not well defined because the region of definition of the input and output are no longer one to one in frequency space. In a linear system the magnitude of the transfer function, $H_{yx}(f)$, with y(t) as input and x(t) as output, is the reciprocal of the previously defined transfer function, $H_{xy}(f)$; that is,

$$H_{xy}(f) = \frac{1}{H_{yx}(f)} . \tag{15}$$

In a nonlinear system, there is an additional dependence on the correlation function, the coherence, such that (Bendat and Piersol, 1966)

$$H_{xy}(f) = \frac{\gamma_{xy}^{2}(f)}{H_{yx}(f)} . \tag{16}$$

A second-order statistic of a time series is bispectrum, which when normalized gives bicoherence, $B(f_1,f_2,f_1+f_2)$ (Hasselman et al., 1963; Haubrich, 1965). Bicoherence is defined as

$$B(f_1,f_2,f_1+f_2) = \frac{\left|\frac{1}{n}\sum_{j=1}^{n} x_j(f_1)x_j(f_2)\,x_j^{*}(f_1+f_2)\right|}{\frac{1}{n^3}\sum_{j=1}^{n} x_j(f_1)x_j^{*}(f_1)\sum_{j=1}^{n} x_j(f_2)x_j^{*}(f_2)\sum_{j=1}^{n} x_j(f_1+f_2)x_j^{*}(f_1+f_2)} \tag{17}$$

which can be used as a measure of nonlinearities of a single time series. It can distinguish orderly deviations of a signal from a sinusoid. It two frequencies, f_1 and f_2, plus their sum, are consistently associated, then the bicoherence will be large; otherwise, their relative occurrence should be uniformly distributed and, therefore, poorly correlated.

Digital sampling of all time series was done at a time increment, Δt, of 0.812 second, which gave a nyquist frequency, f_n, of 0.62 hertz, i.e., period of 1.2 seconds. It was verified that this nyquist frequency was sufficiently high to minimize any effect resulting from aliasing. Total record length used was uniformly 13 minutes, 42 seconds. The incremental frequency band width, Δf, was 6.2×10^{-3} hertz. The number of data points used was one thousand; maximum lag was one hundred points, i.e., 81.2 seconds.

Auto- and cross-spectral analyses were made using a BioMedical Time Series program (BMDO2T). Comparison of spectra obtained from this program with spectra obtained from other programs which used the Fast Fourier Transform of the original signal verified the fact that the BioMedical program was sufficiently capable of isolating all pertinent spectral features of our data.

DISCUSSION OF RESULTS

SWASH DYNAMICS

Analytical Description

The one-dimensional nonlinear first-order wave equations are written as

$$\frac{\partial h}{\partial t} + \frac{\partial (hu)}{\partial x} = 0 \tag{18}$$

and

$$\frac{\partial u}{\partial t} + u \frac{\partial u}{\partial x} + g \frac{\partial (h - h_o)}{\partial x} = 0 \tag{19}$$

where u is horizontal component of velocity, h_o is undisturbed water depth, h is water depth behind the bore face, and $(h - h_o)$ is an index of the strength of the bore (see Fig. 5). These equations denote conservation of horizontal mass and momentum, respectively.

Using these equations, Shen and Meyer (1962) developed an analytical partial description of the swash process. In their solution major dynamical variables were organized into canonical variables, in terms of which the basic equations were rewritten and solved using the method of characteristics.

In the time-space domain, the swash cycle begins at $t = 0$ and $x = 0$, which is when the bore reaches the original shoreline. At $t = 0$ there is a singularity of the solution, indicating coincidence of the bore location and the shoreline. It is at this point that the bore collapses. Collapse indicates the disintegration of the bore configuration. After collapse, i.e., for $t > 0$, two limiting characteristic lines occur: (1) one which defines the location of the leading edge, i.e., the moving shoreline, and (2) one which occurs only during the latter part of the backwash and defines the location of a bore front.

The characteristic in the x,t plane which defines the location of the leading edge is given by

$$x_s(t) = u_o t - \frac{\gamma t^2}{2} \tag{20}$$

where

$$\gamma = g \tan \beta \tag{21}$$

and β is the angle the beach slope makes with horizontal.

Note the similarity of Equation 20 to the well-known relation of a simple projectile which moves, without friction, on a fixed slope, β. The last term on the right side of the equation denotes deceleration resulting from gravity. To illustrate the similarity, the equation of motion for a unit mass moving up an incline is given by $d^2(s(t))/dt^2 = -g \sin(\beta)$, which can be solved to give

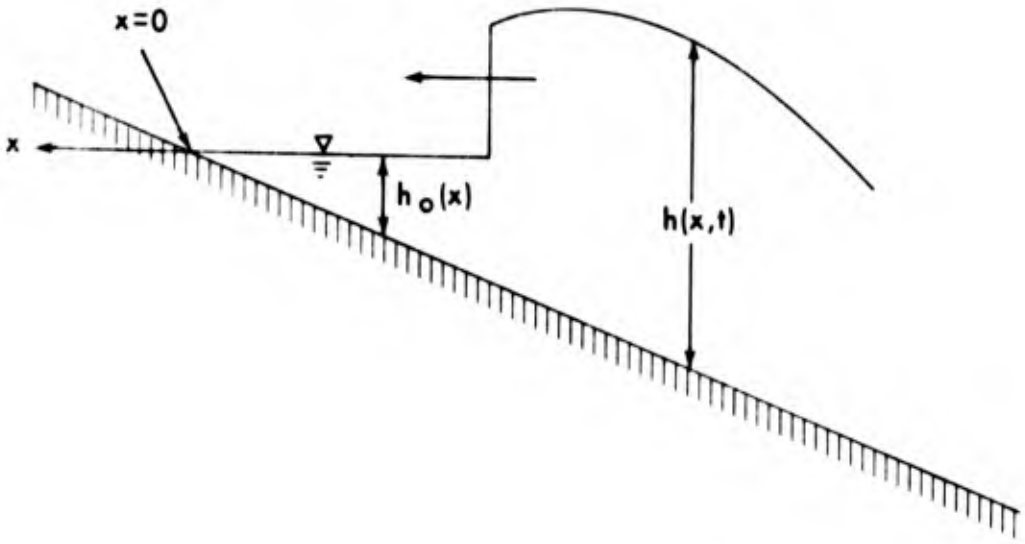

Figure 5. Bore configuration and associated symbols. This bore has yet to reach the shoreline, x = 0.

$s(t) = v_o t - g \sin(\beta)\, t^2/2$, where $s(t)$ is upslope displacement and $v_o = (d\, s(t)/dt)_{t=0}$. For small slope, i.e., $\beta \leq 20°$, $v_o = u_o$, $\sin(\beta) = \tan(\beta)$, and $x(t) = s(t)$. Thus the integrated equation of motion can be rewritten as $x(t) = u_o t - (g \tan(\beta)/2)\, t^2$, which is identical to Equation 20. Note that in both equations the movement of the leading edge or a unit mass is uniquely described by initial velocity, u_o, and the slope, β, which is assumed constant.

In the vicinity of the leading edge and at a fixed time, swash depth is approximated by

$$h = \frac{(x_s(t) - x)^2}{(3t)^2} \quad . \tag{22}$$

Substituting from Equation 20, Equation 22 can be rewritten as

$$h = \frac{[(u_o t - \gamma t^2/2) - x]}{9t^2} \quad . \tag{23}$$

Thus, swash configuration is also completely described as a simple function of initial speed, u_o, and beach slope, β.

Assumptions necessary for these mathematical solutions are as follows: (1) a single swash cycle is completed without interference of successive input waves, (2) the original bore travels into water at rest, and (3) the beach slope is constant.

A typical example of frequently observed configurations of h(x,t) relative to the local surface is given in Figure 6a. Progressive thinning of the swash mass occurs in conjunction with upslope movement of the leading edge following initial collapse of the incoming wave at the shoreline. During backwash, thinning continues

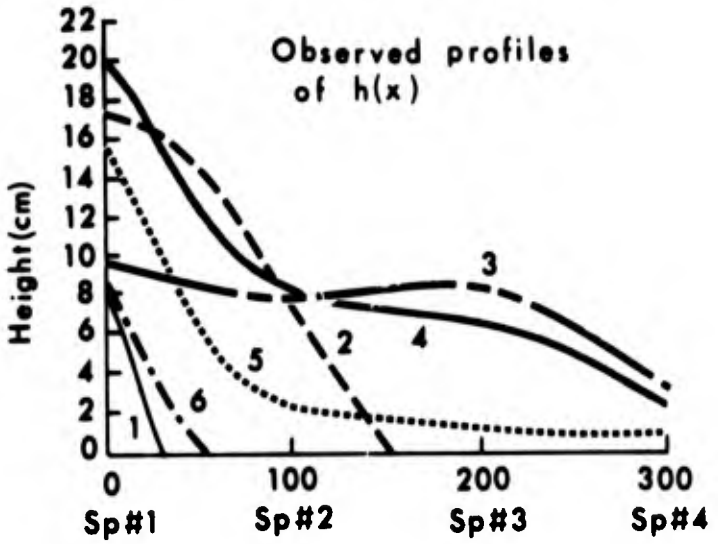

Figure 6a. Observed across-beach profiles of swash depth relative to the sand surface during a complete swash cycle.

on the upper portion of the beach, and a secondary maximum develops on the lower swash slope. This secondary maximum was associated with either a retrogressive bore or a collision between successive swashes.

Theoretical values of h(x,t) are given in Figure 6b. These predict that, after reaching the initial shoreline, the profile sequentially deviates from the bore configuration by thinning of the swash mass. However, thinning continues from bore collapse throughout the entire swash cycle, thus failing to predict a secondary maximum, as observed. This discrepancy results from the fact that the input waves were periodic, whereas the theory assumed a solitary input wave.

Figures 7a and 7b represent time-history plots of swash depth at positions of the four across-beach swash probes. Sequential arrival of the leading edge and the propagation of swash maxima in the upbeach direction is noted. At each station the initial rise of swash depth is more rapid than the subsequent decrease.

In both figures, the lower beach stations exhibited a second maximum during the latter portion of the swash cycle. In Figure 7a, the second maximum is initiated at midbeach and propagates downslope while increasing in relative magnitude. This is a common feature and is similar to the retrogressive bore which Shen and Meyer suggested. The second maximum shown in Figure 7b behaved differently. The second maximum occurs on the lower beach and propagates upslope. This feature was associated with overriding of a succeeding swash before completion of a previous swash cycle and is a typical condition resulting from periodic input waves. As shown in Figure 7c, the theory fails to predict the double maxima. However, the observed swash configurations showed a reasonable degree of qualitative agreement with predictions using the Shen and Meyer theory during the uprush and the initial part of the backwash.

If it is assumed that the leading edge is described by Equation 20, then, by

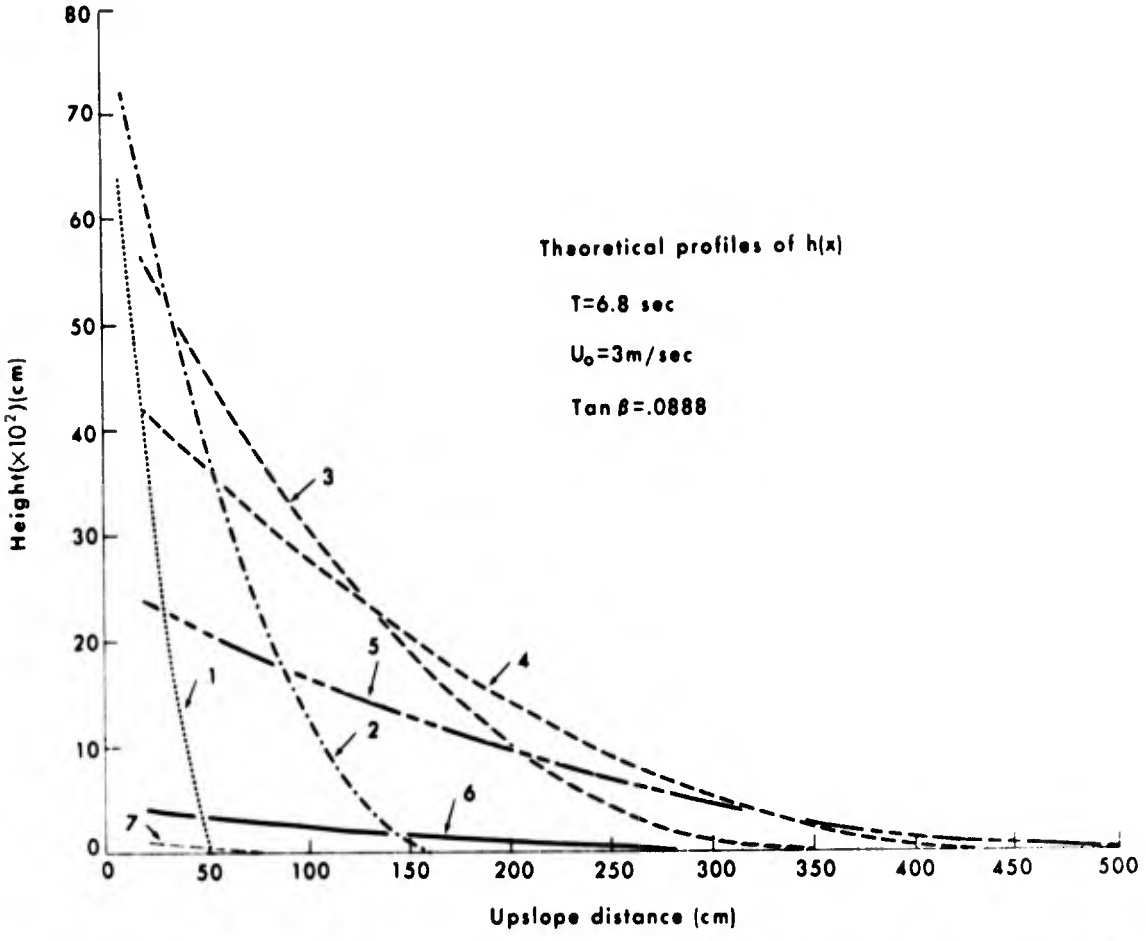

Figure 6b. Theoretical across-beach profiles of swash depth relative to the sand surface during a complete swash cycle.

letting $x_s(T) = 0$, for $T > 0$, the duration of the swash cycle is given by

$$T = \frac{2u_o}{g \tan \beta} . \tag{24}$$

Assume that the input wave, a bore, has a celerity given by

$$c = [g(h = H)]^{1/2} \tag{25}$$

where h_o is undisturbed water depth and H is the bore height (Wiegel, 1964). At the shoreline, $h_o \to 0$, this becomes

$$C = (gH)^{1/2} . \tag{26}$$

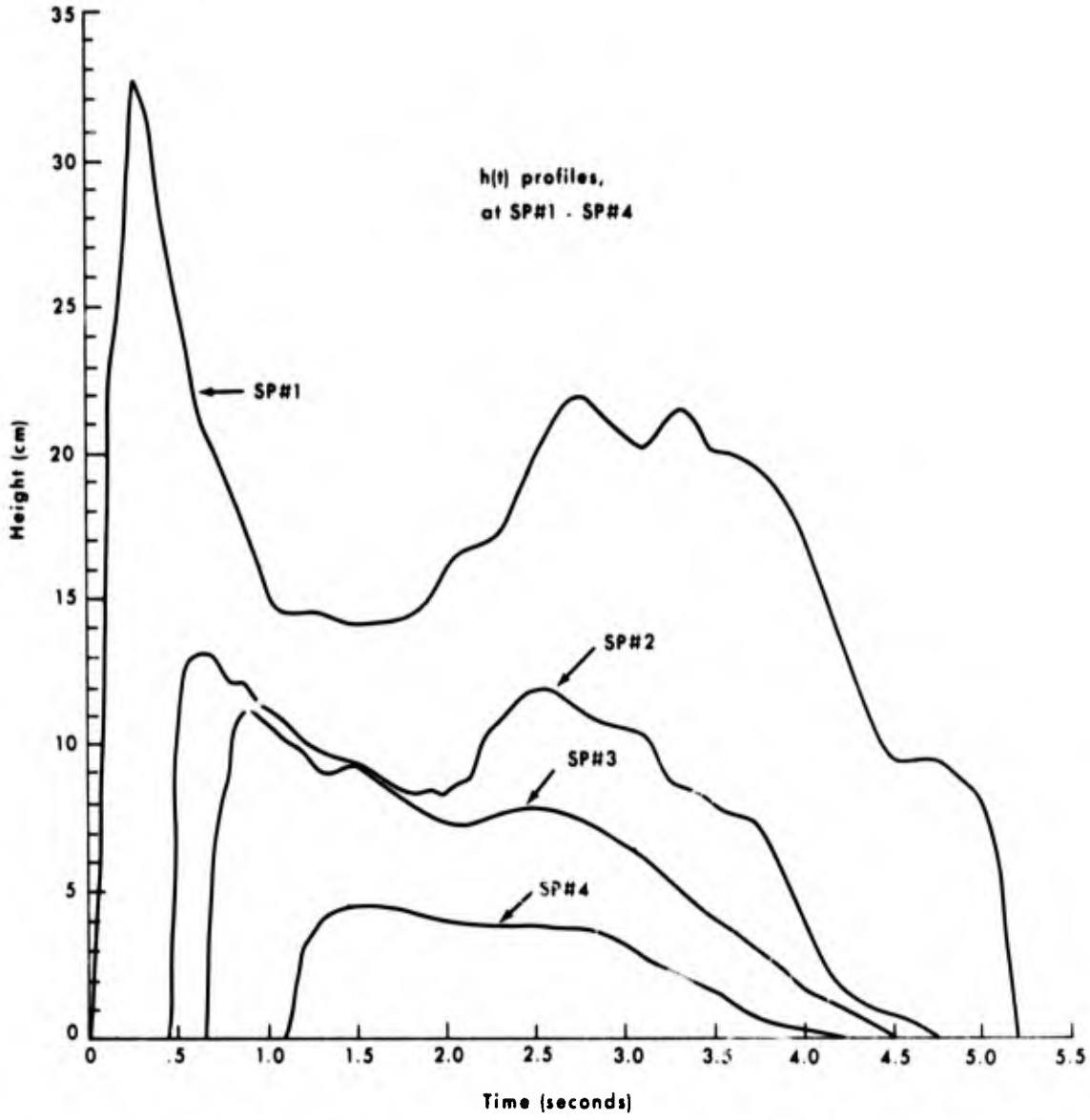

Figure 7a. Observed time history of swash depth for several across-beach stations. Note feature similar to a retrogressive bore which forms on the lower beach during the latter portion of swash cycle.

The relationship between celerity and particle velocity in a bore is not known. Let us assume

$$u_o = AC \tag{27}$$

where A is a constant. Substituting Equations 26 and 27 into 24 yields

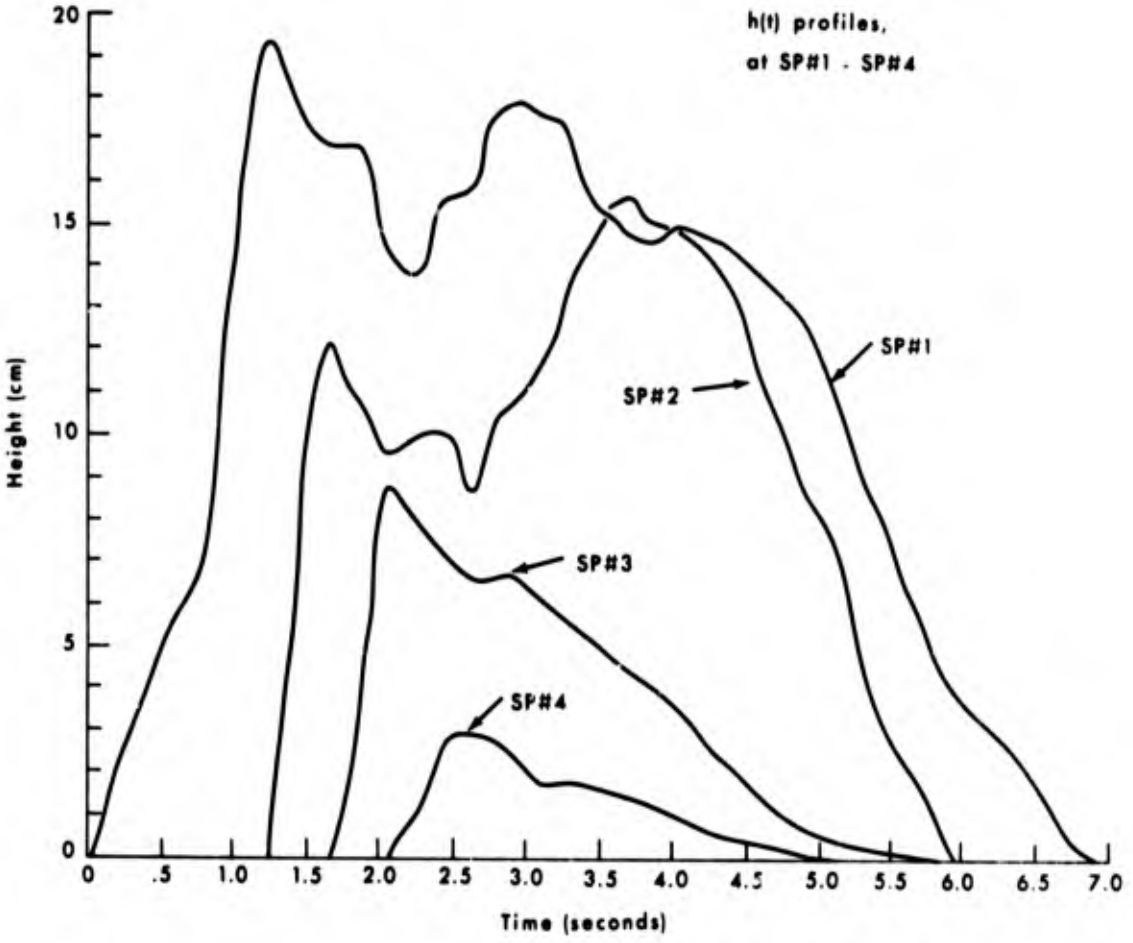

Figure 7b. Observed time history of swash depth for several across-beach stations. Note overriding of a succeeding swash on the lower beach during the latter portion of swash cycle.

$$T = \frac{2\,A\,H^{1/2}}{g^{1/2}\,\tan\beta} \tag{28}$$

or

$$f = 1/T = \frac{g^{1/2}\,\tan\beta}{2\,A\,H^{1/2}} \quad . \tag{29}$$

A plot of observed values of f versus H is given in Figure 8 on the basis of measurements from one hundred individual waves at SP #2 for a constant slope. Equation 29 gives the best fit with the data if "A" is taken to be 3.4. In a breaking wave the particle is generally equal to celerity; therefore, the value A = 3.4 is higher than expected.

It should be noted that Equation 26 estimates the celerity, which is only reflective of potential energy of the wave prior to breaking. As the wave breaks, both potential and kinetic energy of the wave are released to produce the initial momentum, which must be larger than values estimated solely from potential energy. The value A = 3.4 is possibly a result of this mechanism.

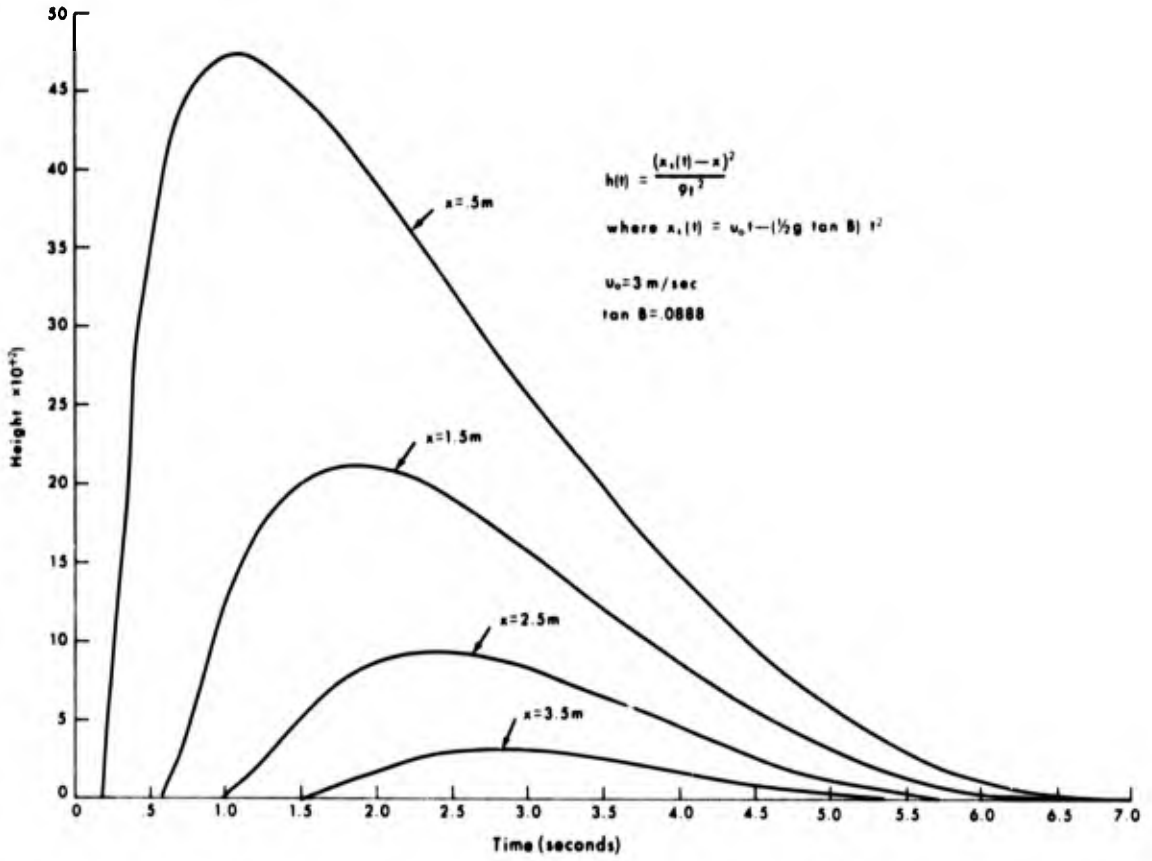

Figure 7c. Theoretical time history of swash depth for several across-beach stations. Locations, x, used to evaluate h(x,t) correspond to approximate locations of the instruments during data runs. Notice that only one peak occurs as a result of uprush.

The swash duration defined in Equation 24 represents the period during which the sand at the base of the slope remains inundated. The observed inundation periods agreed with the periods predicted from Equation 24 by at least 30 percent and most often within 15 percent.

Stochastic Description

An example of the multiple channel field data of swash and ground water is given in Figure 9. From the bottom to the top of the figure, there is an upbeach sequence of output from probes SP #1 through GW #2. For instance, referring to the water level trace at x = 2 meters, SP #3, the sequence of events is as follows: At t = 2 seconds sand surface was exposed; at t = 3 seconds a swash mass inundated the station, water quickly reaching a maximum depth; a much slower decrease followed until about t = 11 seconds, when the sand surface became exposed again.

Several characteristics of these traces associated with swash can be distinguished. In an upslope direction, (1) duration of local inundation decreases, (2) maximum water depth decreases, and (3) water level traces tend to be more regular and smooth.

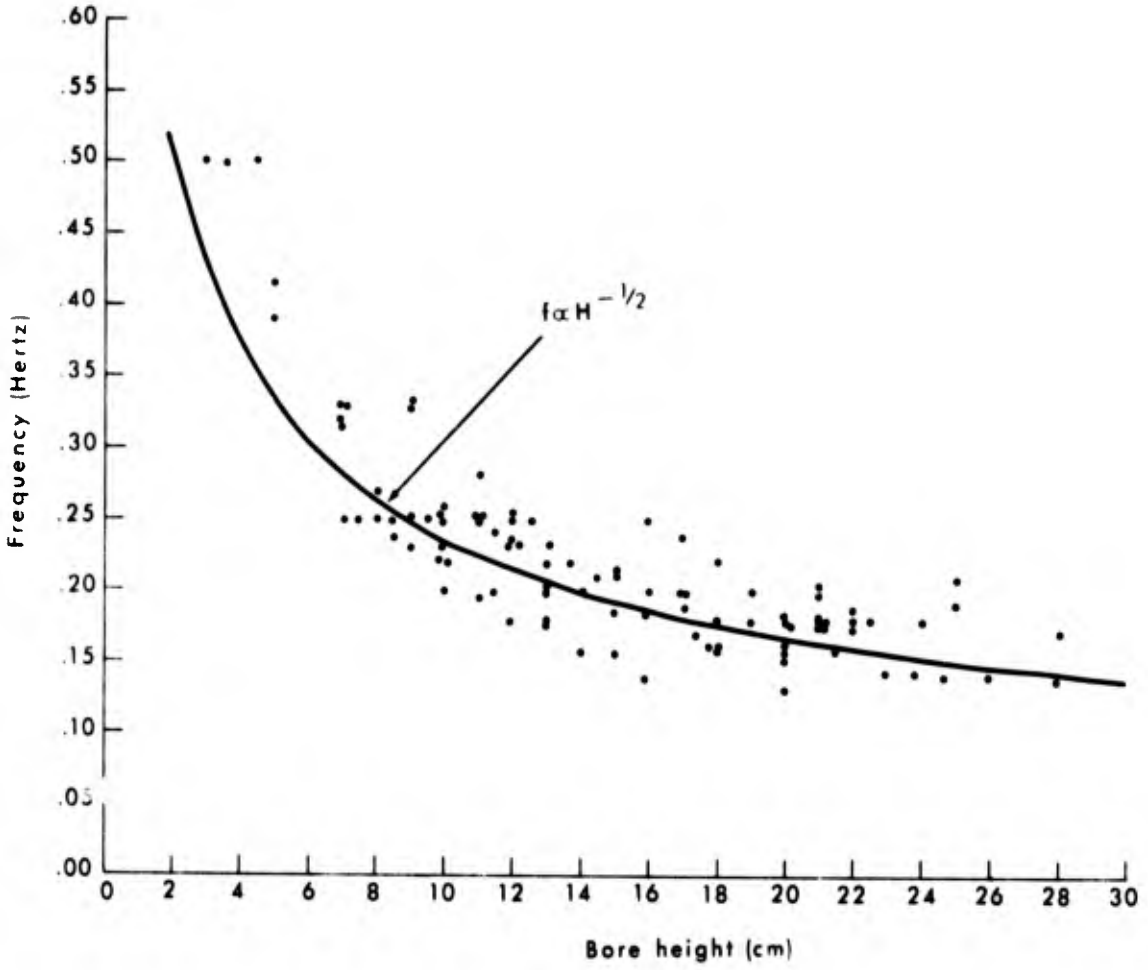

Figure 8. Swash frequency as a function of bore height. Height and period for one hundred swashes during Run #1 are plotted.

Figure 10 is an example of the across-beach sequence of power spectra. Note a progressive decrease in total and peak spectral power up the swash slope. Relative power attenuation was consistently greatest at the higher frequencies, indicating that the beach slope acted as a low-pass filter on the swash. Localization of the high-frequency spectral peak, B_1, on the lower portion of the beach slope suggests sources for this variability: (1) retrogressive bore associated with the individual swashes, which can generate the double peaked profile of h(t), and (2) collision between successive swashes, giving rise to abbreviated swash cycles and secondary disturbances (see Figs. 7a, b, c). Both processes can produce high-frequency fluctuations in swash profiles and are characteristic of the lower region of the beach.

The most dominant spectral peak, B_2, was at the frequency associated with the interval between arrival of successive swashes. It is important to distinguish between this interswash period and local inundation period. Interswash period denotes the time interval between successive swash peaks at a given station on the beach slope. This is not necessarily equal to input wave period because some waves fail to produce swash as a result of attenuation from collision with a preceding swash at the lower beach. Inundation period is the time a given location

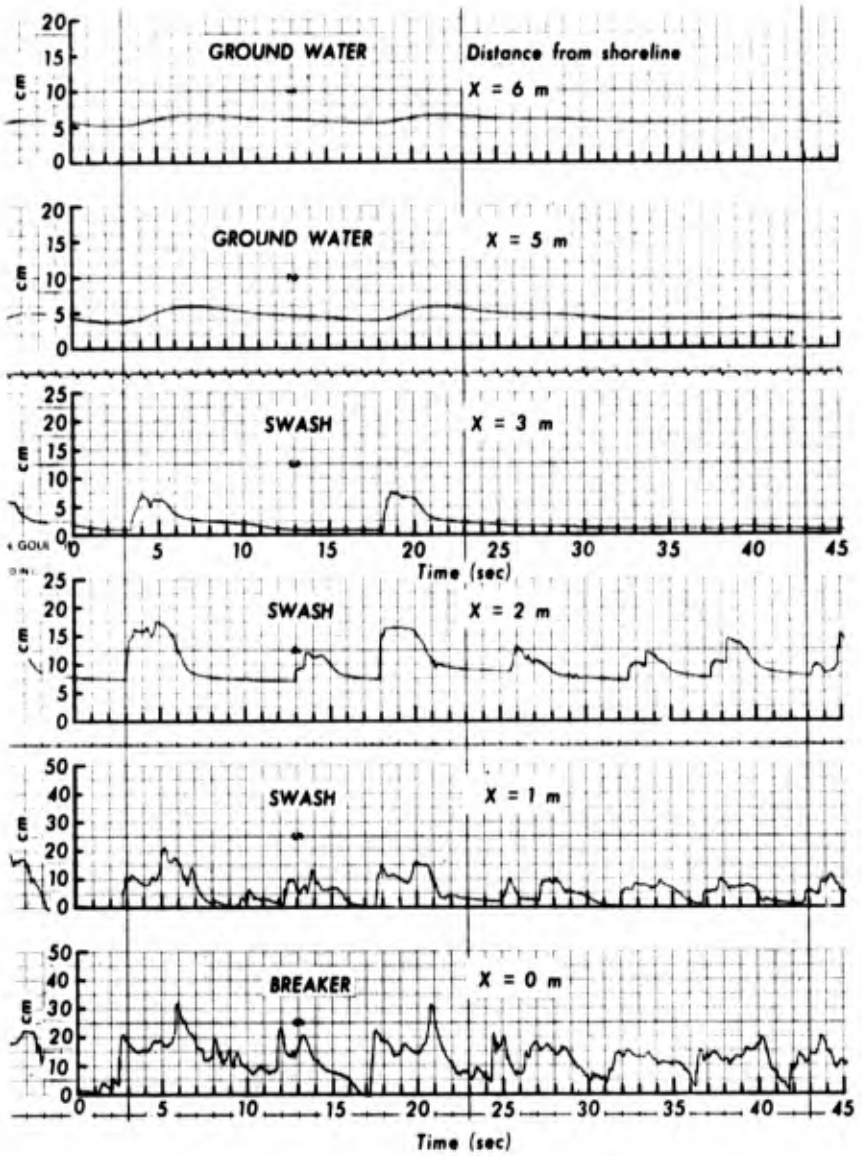

Figure 9. Examples of sample functions for SP #1 - SP #4 and GW #1 - GW #2.

remains under water; it is generally smaller than the interswash period. Local inundation period generally decreases up the beach slope (Fig. 11).

The narrow band width of B_2 in Figure 10 was due to the uniformity and regularity of the interswash period during this data run. If the interswash period had displayed considerable variance, the band width of the power peak would have increased. This in turn would have decreased the magnitude of the peak owing to a wider distribution of the given variance.

Battjes (1971) showed that the family of Rayleigh distribution functions closely approximates the frequency of occurrence of run-up heights. On a given beach slope, upslope excursion is directly proportional to run-up height, and both

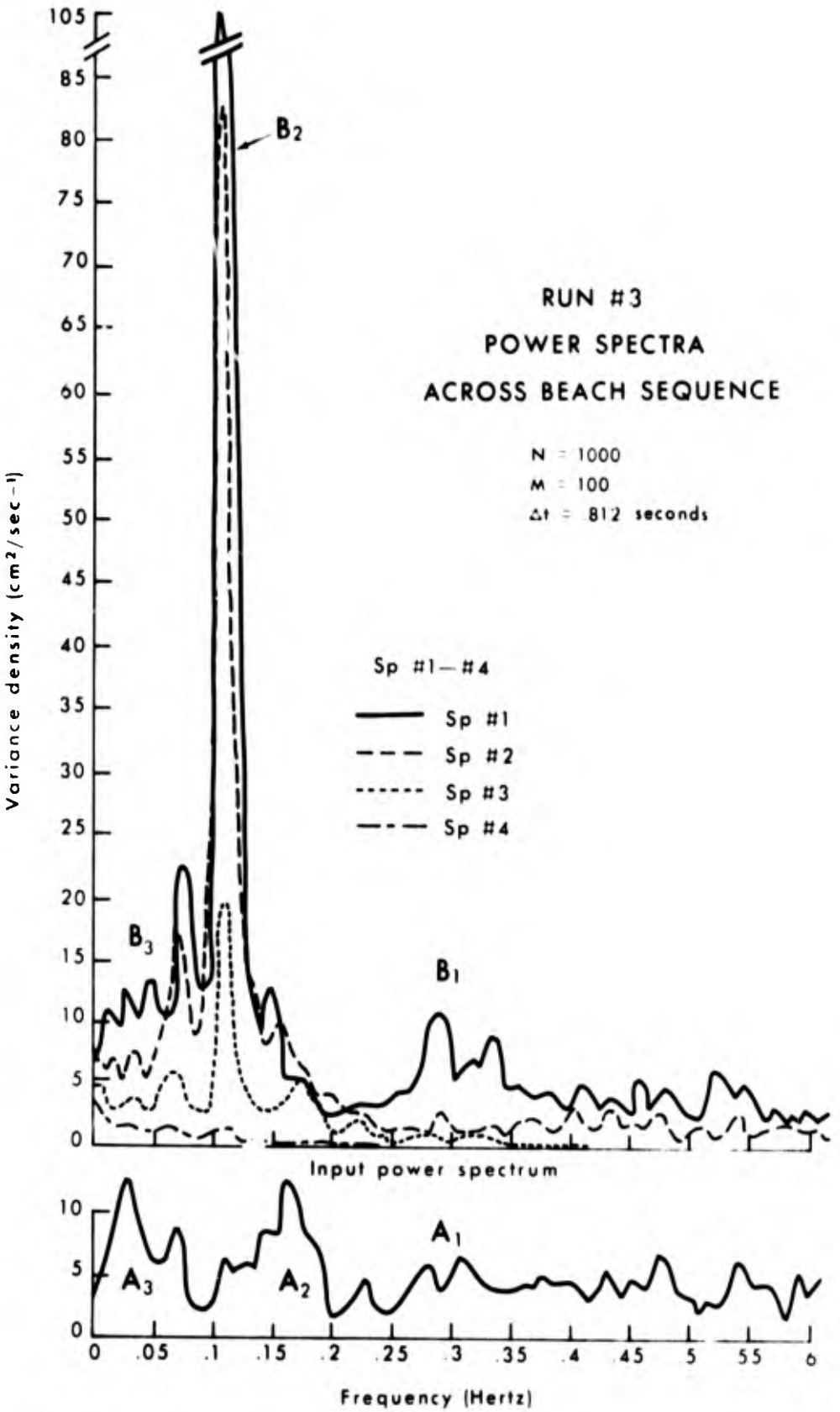

Figure 10. Across-beach sequence of power spectra for input waves and four swash probes. Notice the consistency of the dominant swash period.

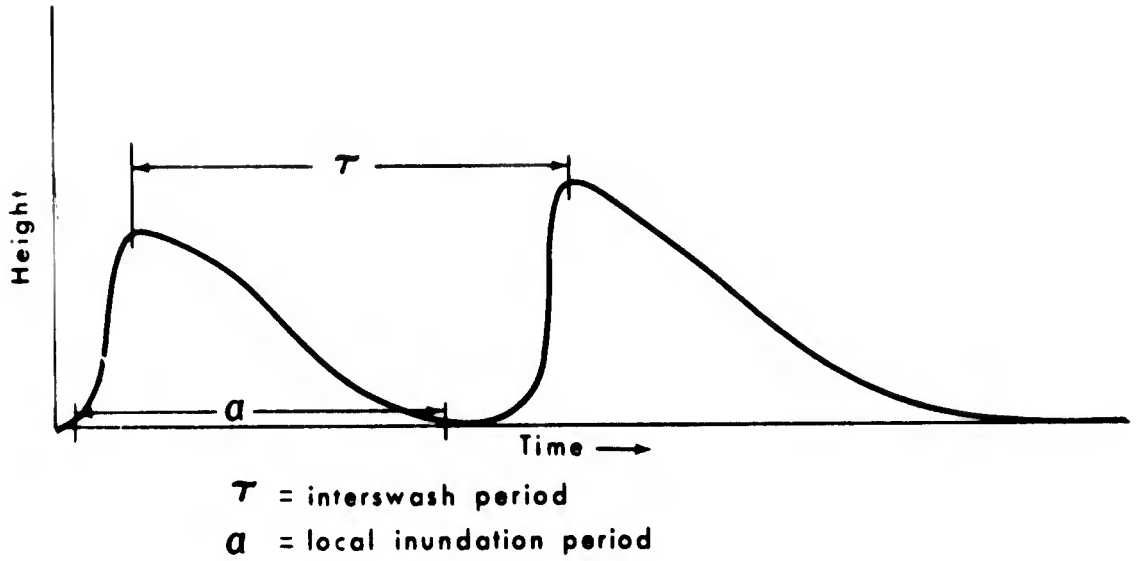

Figure 11. Distinction between interswash period, τ, and local inundation period, α, is illustrated.

parameters can be shown to be Rayleigh distributed. The excursion distribution predicts a systematic decrease in the number of swashes reaching successive upslope positions. Because of this across-beach decrease in swash excursion, one must expect a lengthening of the interswash period up the swash slope. In frequency space, this situation should be reflected by an expansion of spectral peak, B_2, into lower frequencies in an upbeach direction. However, these data, as shown in Figure 10, failed to yield evidence to support this expectation. One possible explanation for the lack of support for Battjes' derivation is that, for the beach slope and wave conditions which existed when these data were taken, rapid attenuation of swash excursions was confined to a narrow region very near the run-up limit upslope of the highest swash probe on the beach face.

Lack of shift in B_2 upslope is also evident in Figures 12 and 13, which are spatial-frequency plots of variance (power) density. Figure 12 represents Run #3, and Figure 13 represents Run #6.

The magnitude of input wave energy at the shoreline increased greatly between Run #3 and Run #6, as indicated in these figures. This increase in energy was not produced by a change in offshore wave field but was associated with the tidal rise in water level during Run #6, which allowed waves to reach the shoreline with reduced attenuation as a result of breaking on the bar. Increased water depth also produced a shoreward displacement of the breakpoint. As a result, the location of the swash slope spectral peaks showed a similar shoreward displacement. However, their locations relative to the breakpoint remained approximately the same for both runs. The basic pattern of the distribution of variance density on the swash slope also remained consistent from Run #3 to Run #6.

The increase in input wave energy at the shoreline in Run #6 was reflected in an increase in power of wind waves, A_1, and input swell, A_2, particularly the latter, but not in the spectral intensity of A_3, which remained essentially unchanged between Run #3 and Run #6.

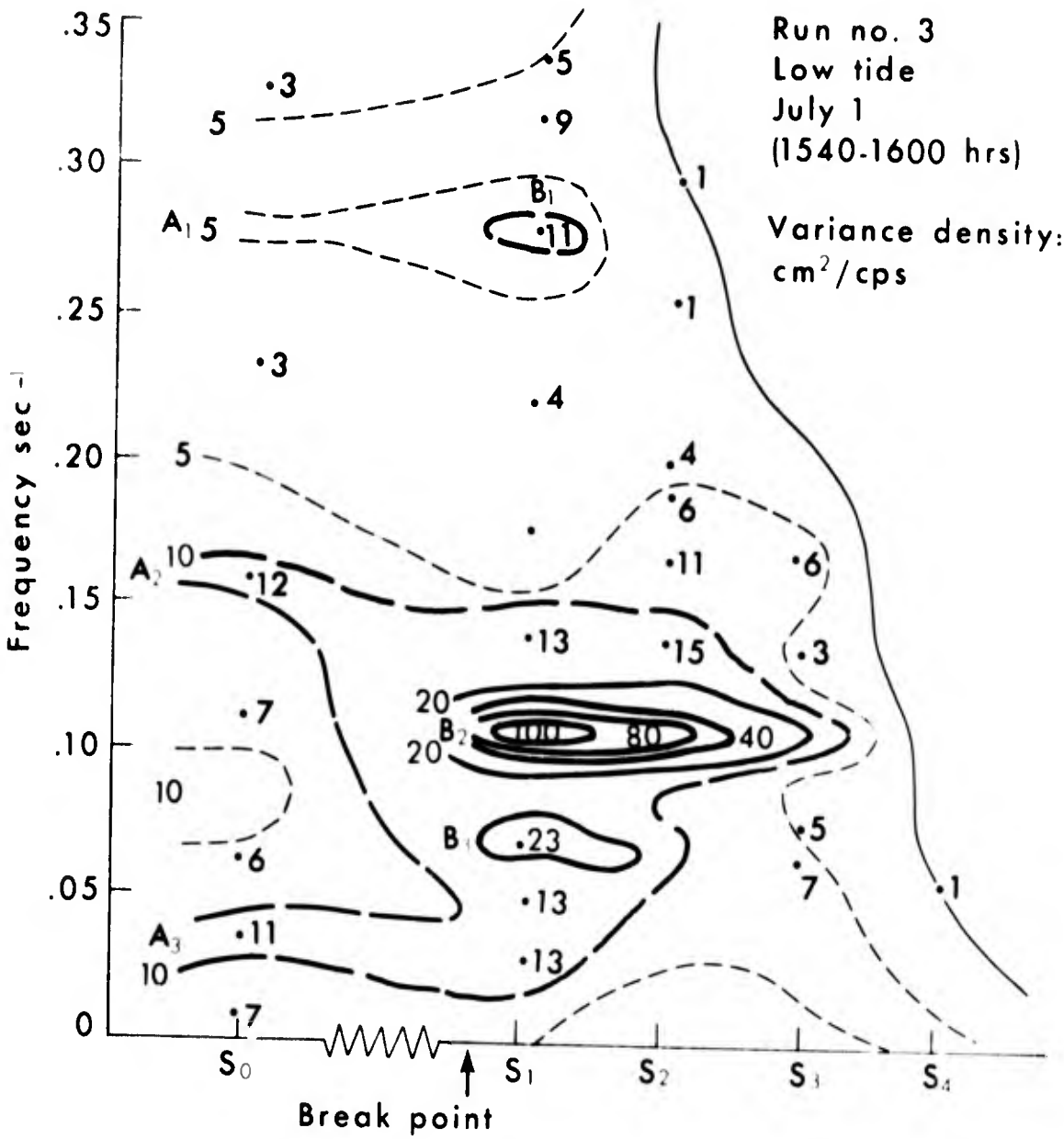

Figure 12. Plot of variance density (Run #3) as a function of space and frequency, i.e., $P_x(x,f)$.

Associated with this increase of input wave energy was an increase in total power under the major swash peak, B_2, and secondary peak, B_1. It is important that the increase in power content of B_2 occurred in terms of greater band width rather than in terms of greater peak power, which remained essentially unchanged. An explanation of this is that with increased input wave energy there was an increase of mass in each swash, causing an increase in swash depths and hence an across-beach lengthening of the local inundation period. These changes in individual swashes in turn caused a greater degree of interaction between successive swashes, resulting in increased variation of the interswash period. This caused spreading of power over a wider frequency band.

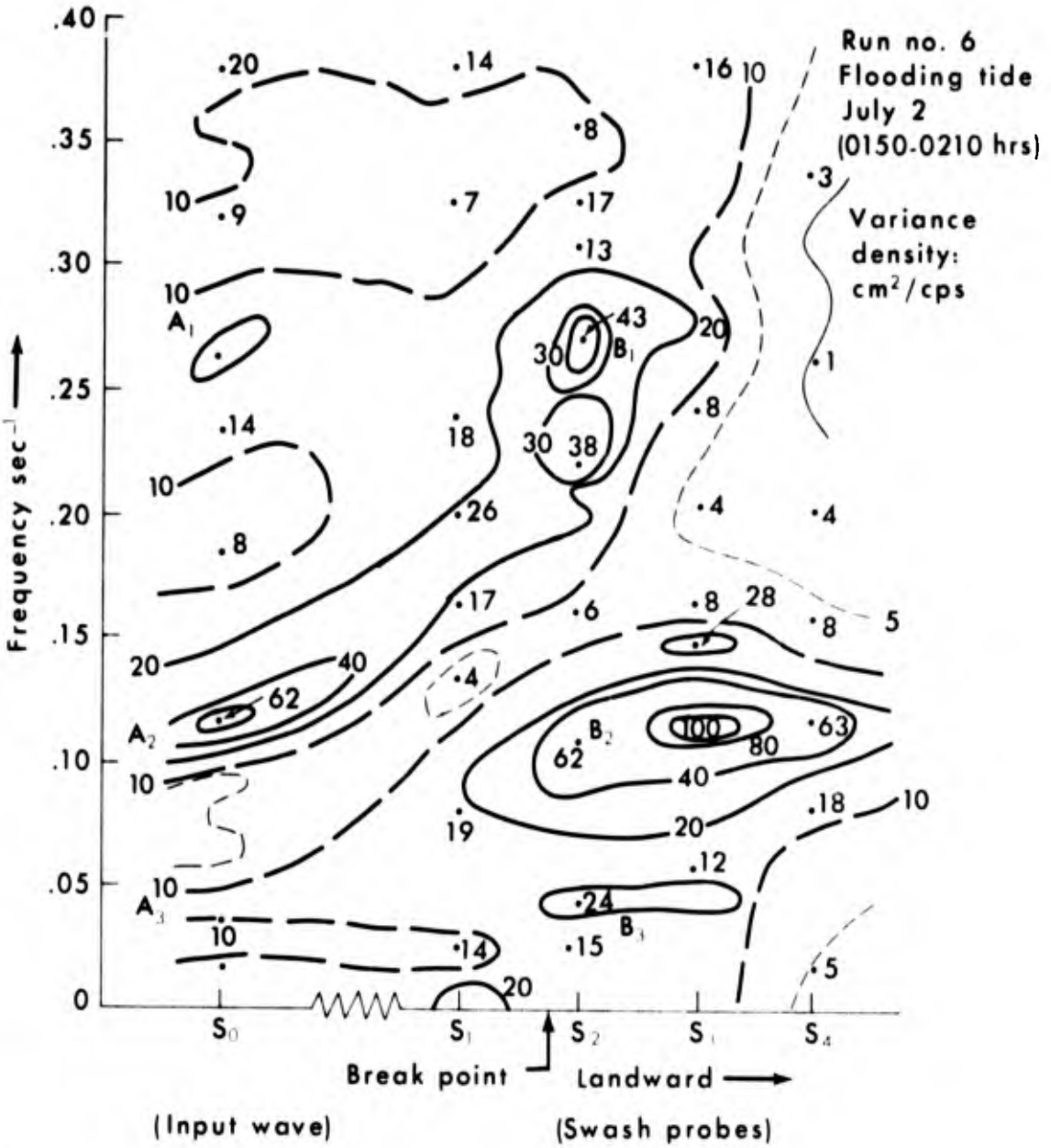

Figure 13. Plot of variance density (Run #6) as a function of space and frequency, i.e., $P_x(x,f)$.

The increased interaction between successive swashes should also have given rise to more high-frequency fluctuations in swash depth. This was observed inasmuch as spectral peak, B_1, was greatly increased during the flooding tide (Run #6) although there was only a minimal increase in the input power in this frequency band, A_1. Further evidence for this effect is that B_1 was limited to the lower portion of the beach, where interactions between swashes are concentrated.

The fact that input waves, A_2, produced responses, B_2 and B_1, of different frequencies indicates that the transformation of energy across the breakpoint was a nonlinear process.

As indicated previously, nearshore water level fluctuations exhibited low-frequency beat components, A_3 (see Figs. 10, 12, and 13). The power content in this low-frequency region remained essentially unchanged between Runs #3 and #6. Munk (1949) was first to recognize a beat oscillation in the range of about 1 to 5 minutes in the nearshore wave field; his observation was followed by that of Tucker (1950), who noticed that this phenomenon, called surf beat, was associated with grouping of high and low waves in the incident wave train. Longuet-Higgins and Stewart (1962) later explained that the slow rise and fall of mean sea level in surf beat was in balance with the variations in radiation stress in shoaling waves.

If beat frequencies recognized in the present data are the same as surf beat, the bicoherence of incident wave records should reveal nonlinear interactions between spectral peaks, as indicated by Hasselman et al. (1963). Calculation of bicoherence for these wave data for all data runs failed to indicate any such evidence. In fact, these observed low-frequency fluctuations retained almost identical spectral characteristics despite two different input wave conditions at the shoreline, i.e., one having small wave heights near the shoreline owing to breaking over the inner bar (Run #3) and the other having increased wave height near the shoreline owing to reduced breaking over the inner bar (Run #6). The implication is that these long-period fluctuations in the data were not directly affected by incident wave characteristics or degree of breaking.

Examination of cross-spectral characteristics between S_o and SP #1 indicates the possible nature of A_3. As shown in Figure 14, at low frequencies near A_3 there was high coherence but virtually no phase lag between the two time series, suggesting the presence of a standing wave with its antinode located at the shoreline. If the input wave probe, S_o, and the swash probe, SP #1, were both located within a quarter of a wavelength of the shoreline, one should expect a zero phase lag. If these waves were essentially linear (sinusoidal), then one would expect high coherence. Previously, Sonu (1973) reported beat oscillations in rip velocities which could be explained as resulting from a standing wave near the shoreline; in that case the velocity lagged $\pi/2$ behind surface fluctuations, as would be expected from a linear theory.

Using linear shallow-water wave equations, Suhayda (1972) investigated the low-frequency region of the wave spectrum. He showed that for a linear wave field on a sloping bottom the frequency of the standing wave which has a node point x meters offshore is given by

$$f_1 \simeq \frac{2.4\ (g \tan \phi)^{1/2}}{4\pi x^{1/2}} \qquad (30)$$

where x = the distance offshore, and $\tan \phi$ = the bottom slope.

For the range of values of $\tan \phi$ in this study, the frequency to be predicted from Equation 30 is between 0.090 and 0.10 hertz for a standing wave which has a node point 5 meters offshore. For frequencies less than this the two measurements at S_o and SP #1 would be within the same node, and for higher frequencies the measurements would be in adjacent nodes. Thus in this frequency range, f_1, there should be a shift in phase angle from 0 to π.

The observed phase shift in Figure 14, and for two other data runs, occurs at this frequency range. The analysis also indicates a drop in coherence at this frequency, as one would expect from coherence involving a node point in a standing wave

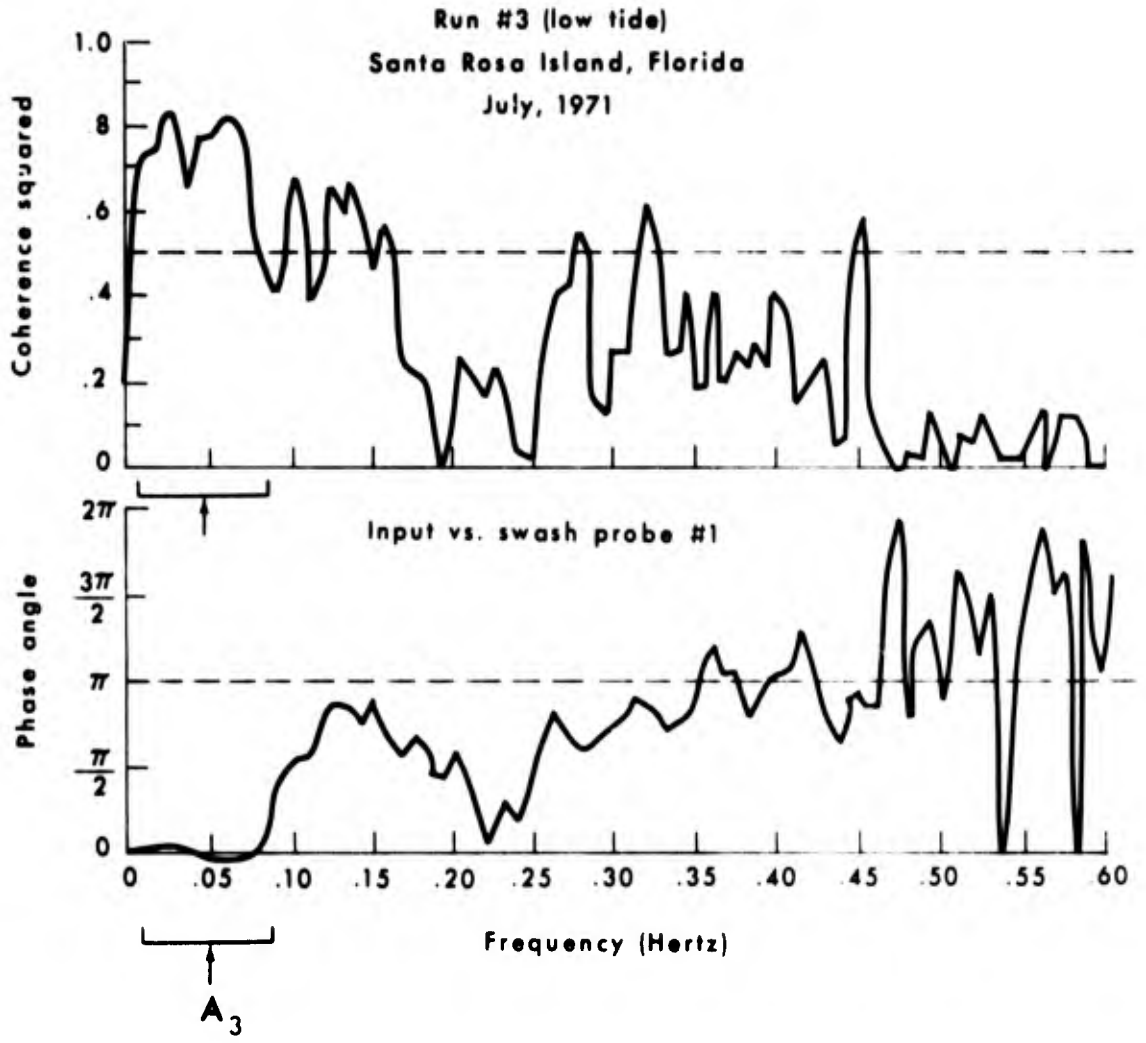

Figure 14. Plot of coherence function and phase angle between the spectra of input waves and SP #1 during Run #3.

field. If it is assumed that all the linear standing waves have approximately the same height, then at this node frequency, f_1, there should be a power minimum. In each case this was observed.

In sum, analysis of the data indicates the important role being played by collision processes in the swash mechanism. This importance has not been identified in past studies based on insufficient resolution of the real phenomena.

INPUT WAVE-SWASH-GROUND WATER INTERACTION

Although input waves are the principal source of energy for the swash, it is a combination of input waves and swash which is the forcing function for high-frequency variations of beach ground water table. The existence of this interaction was suspected by Emery and Gale (1951); however, no attempt has yet been made to explain the dynamic relation either in a conceptual model or on the basis of detailed measurements. In addition to previously mentioned field investigations, numerical

model studies have been conducted (Dominick et al., 1971; Harrison et al., 1971). These focused on prediction of the tidal response of the beach ground water. None have attempted to investigate the high-frequency range, periodicities on the order of several minutes or less, of beach water table fluctuations.

Ground water records (Fig. 9), which were taken at two stations 5 and 6 meters landward of SP #1 and approximately 1 and 2 meters respectively beyond the maximum limit of run-up, indicate that the ground water table exhibited distinct fluctuations with periodicities on the order of 8 to 11 seconds (see spectral peak, C_2, in Fig. 15).

One mechanism which could cause these fluctuations can be identified in Figure 9. Examining the records for GW #1 and SP #1 at time, t, = 2.5 seconds, the leading edge of the swash was located at the base of the slope, x = 0. At the same time the water level in GW #1 was beginning to rise. The concurrence of these two events, (1) initiation of a rise in the water table and (2) the arrival of the swash mass at the base of the swash slope, suggests that a pressure force was transmitted virtually instantaneously through the saturated layer of the beach. This pressure in turn initiated a mass flux which caused the ground water level 5 meters inland to respond.

Although transmission of pressure and associated initiation of mass flux were instantaneous, a lag occurred between the maximum swash depth at the base of the slope and the maximum level of the responding water table. This lag resulted because the mass flux necessary to raise the water table was subjected to frictional retardation in the porous beach matrix. The peak-to-peak lag between SP #1 and GW #1 and GW #2 was less than half a second and could not be clearly isolated.

Water table response to the swash at the base of the slope was consistently observed during every data run. Further evidence of the ground water response is given in Figure 15. In this figure, in addition to the spectral peak C_2, the interswash frequency, another peak, C_3, exists which corresponds to A_3, a beat. As already mentioned, the beat was localized on the lower portion of the swash slope and hence was not evident at SP #2, as seen in Figure 15. However, the beat was transmitted directly into the ground water through the saturated beach face on the lower beach, causing a prominent spectral peak, C_3, at GW #1, which was located far behind SP #3.

As the swash mass moves farther up the beach slope, its exact influence on the ground water cannot be distinguished. However, the records show that the water table in the wells continued to rise as the leading edge of a swash moved up the slope. This indicates that there was a continual influx into the saturated portion of the beach. Once the leading edge passes the point of intersection of the water table and the swash slope, the swash partly infiltrates into the nonsaturated portion of the beach.

During Runs #1-#5, the mean seaward position of the ground water - swash slope intersection was approximately 30-50 cm seaward of SP #4. In Figure 16, examining the location of the water table relative to the surface of the swash slope, it is obvious that near the line of their intersection the two surfaces were in close proximity. Because of this proximity, very little influx of water would be required to cause significant upslope displacement of the location of their intersection.

As an example, during Run #1, if the available pore space constituted 50 percent of the volume of the beach and no water table changes occurred landward of

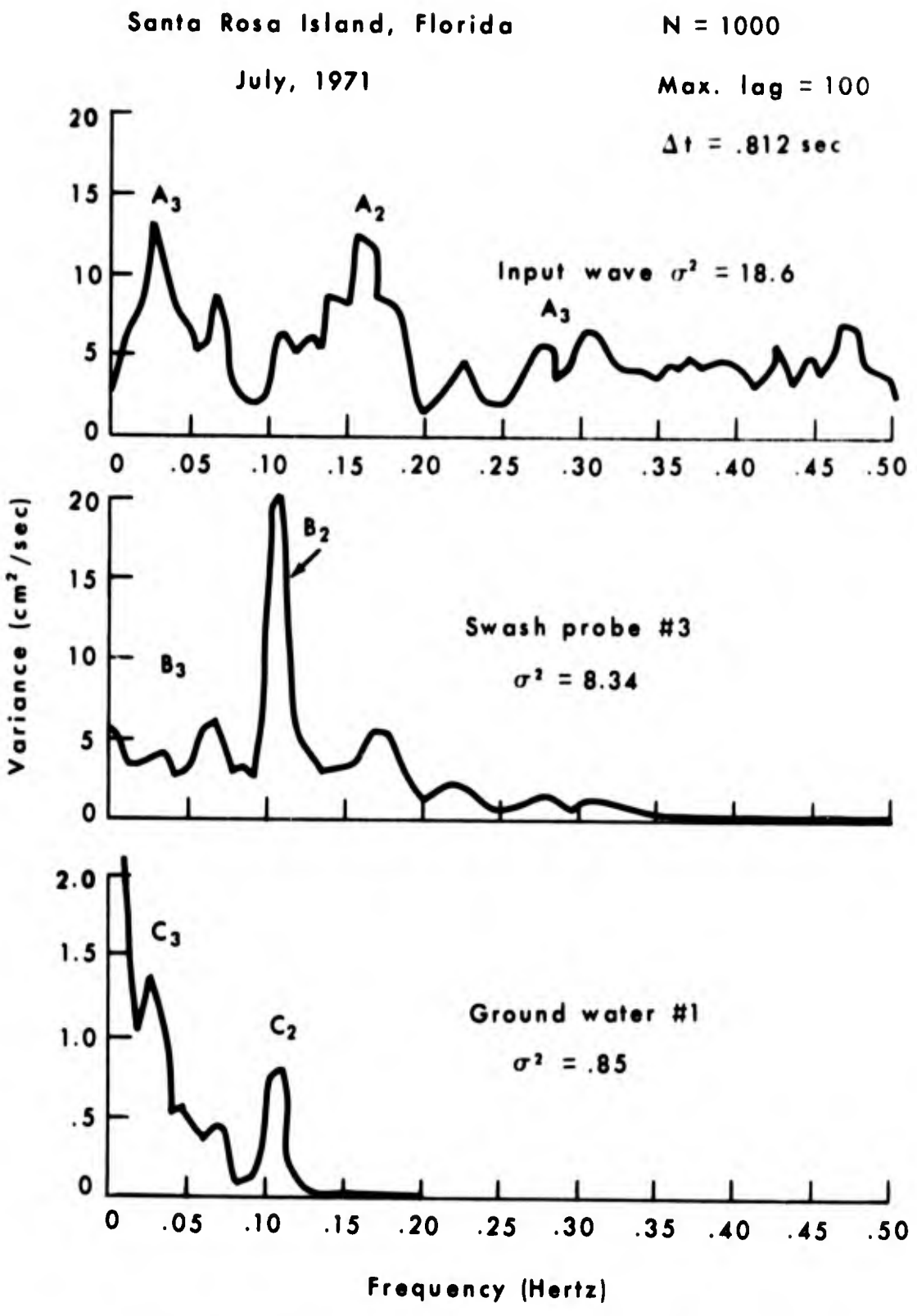

Figure 15. Onshore sequence of power spectra for input waves, S_o, SP #2, and GW #1.

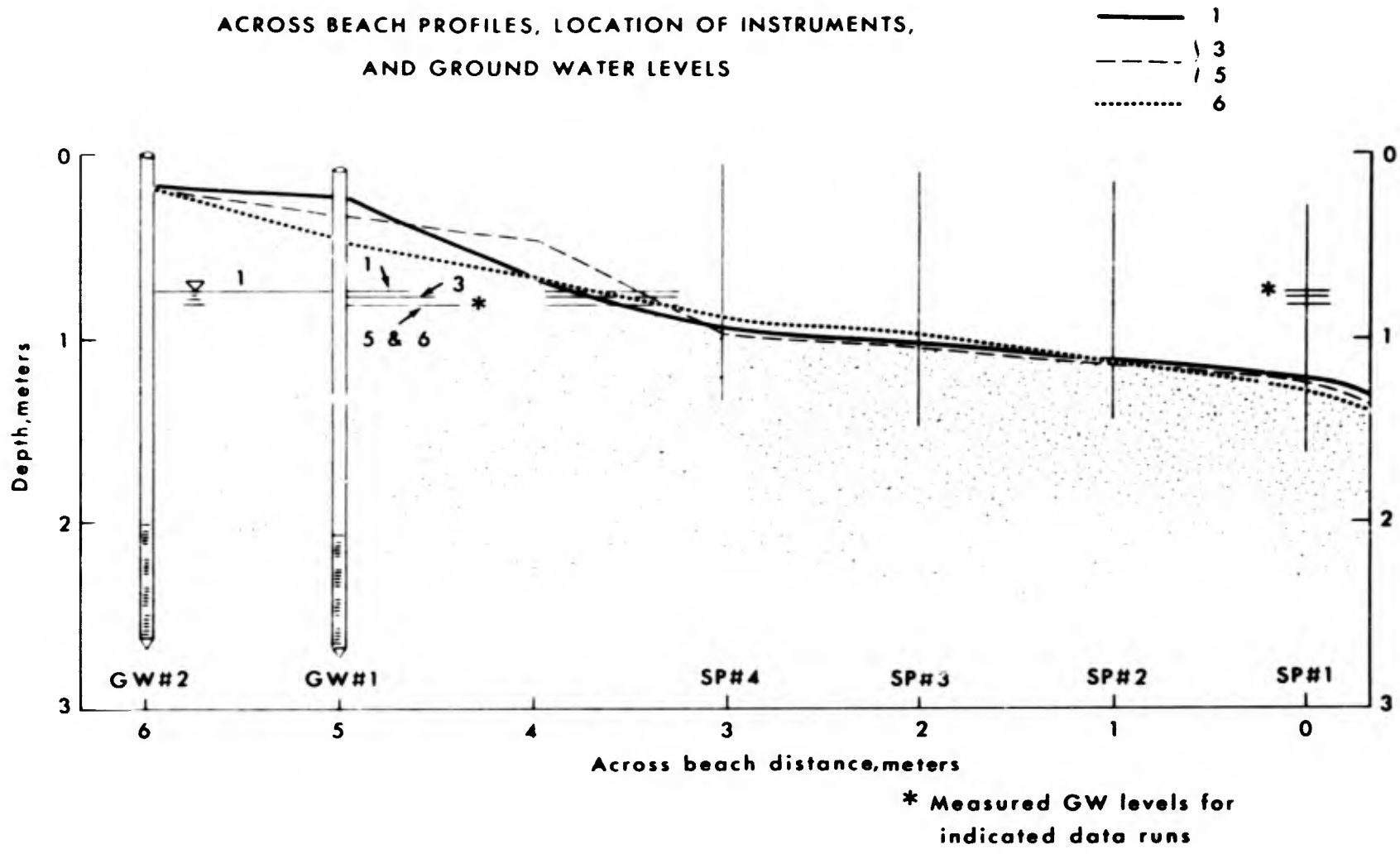

Figure 16. Across-beach profiles, instrument location, and ground water levels. Measured mean ground water levels during each run are indicated (1) at ground water wells, (2) where the horizontal extension intersects the beach slope, and (3) at the toe of the swash slope.

GW #1, then for each centimeter of beach front the addition of approximately 325 cm^3 of water would cause the water table intersection to retreat 130 cm landward; the addition of 150 cm^3 would cause a 100-cm upslope displacement, and the addition of 30 cm^3 would cause a 50-cm upslope displacement. Obviously, very little influx can produce significant upslope migration of this intersection.

Examination of Figure 12 indicates that the power associated with the swash, B_2, was very much greater than the power associated with the low-frequency water level fluctuations, B_3. However, examination of the ground water spectrum in Figure 15 shows that the ground water response to low-frequency fluctuations, C_3, was greater than to swash frequency excitations, C_2. This implies that the beach has the properties of a low-pass filter.

The transfer function representative of this low-pass property is given in Figure 17. Because of the change in the water level during the tidal cycle, GW #1 was closer to the breakpoint in Run #6 than in Run #3. It is evident in Figure 17 that the greater separation from the breakpoint was associated with the red shift of the cut-off frequency as well as the reduction in the amplitude of the transfer function.

Although past studies emphasized much slower excitations, i.e., those of tides, this study indicates that other important fluctuations occur at a much higher frequency. In particular, it is recognized that, because of the low-pass filtering property of the beach matrix, special attention must be given to beat excitations which exist on the lower beach.

BEACH ELEVATION RESPONSE

Swash action produces constant adjustment of the subaerial beach profile. These changes have been examined at differing orders of resolution. The best known aspect of these beach profile changes is that associated with the seasonal wave climate. More recently, the beach change at the tidal periodicity was examined (Sonu and van Beek, 1971), and within-tide changes of beach profiles on an equilibrium profile have been studied and explained qualitatively (Strahler, 1966).

The present investigation examines continuous beach changes. This approach was possible because of both the analog sensing system employed and the stochastic data processing technique. The resulting high-frequency resolution of the changing beach configuration allowed for direct insight into the response mechanism of beach sand levels.

The instrument used in this aspect of the study was a resistance-type water level probe developed at Coastal Studies Institute, Louisiana State University (Truxillo, 1970). The sensing unit consists of (1) a high-resistance lead wire which is spirally wrapped around a threaded PVC rod and (2) a ground which is a stainless-steel tube. When the probe is submerged, the current flows from the lead wire to the ground through the intervening saltwater medium. The higher the water surface intersection on the probe, the less the resistance produced by the lead wire and therefore the less the voltage across the probe. These variations of voltage associated with the changing water level are recorded by an analog strip chart recorder.

Laboratory test of this instrument showed that when the probe was inserted in wet sand the effective location of the maximum voltage which defines the wetted surface occurred at the air-sand interface. Field test indicated that the probe accurately monitored sand surface which remained wetted between successive swashes.

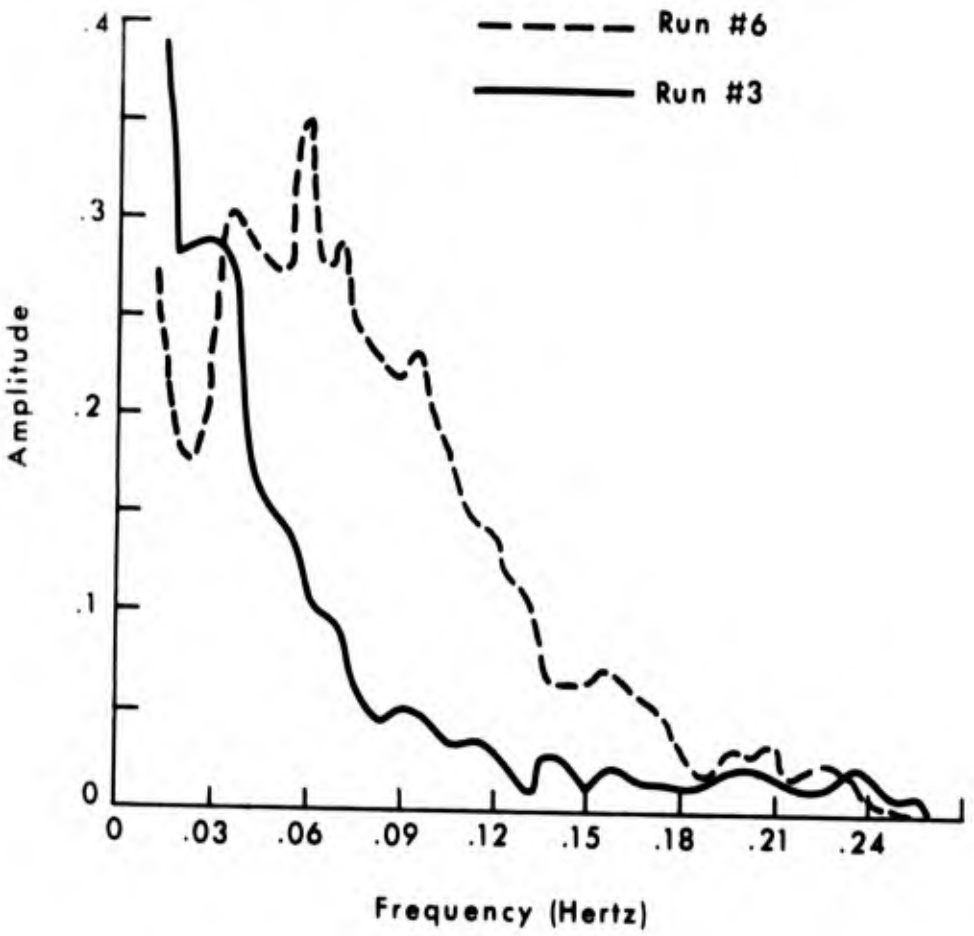

Figure 17. Amplitude of transfer function from input waves to GW #1 during Run #3 and Run #6. Note shift to higher frequencies during Run #6 when breakpoint had migrated upslope.

The performance of the probe was consistent even where the sand on the surface appeared to be only damp in interswash intervals which were as long as a minute and more. During one instance, a stationary probe continuously monitored erosion of as much as 30 cm.

The sand levels were measured at a series of stations across the subaerial beach on a line perpendicular to the local shoreline. The two stations used in this discussion were located 1 meter apart on the upper half of the swash slope. These were chosen because they had adequate swash intervals to allow sufficient exposure time of the sand surface.

Simultaneous time histories of sand level at two stations, as shown in Figure 18, exhibited two distinct features: (1) a quasi-linear trend during an

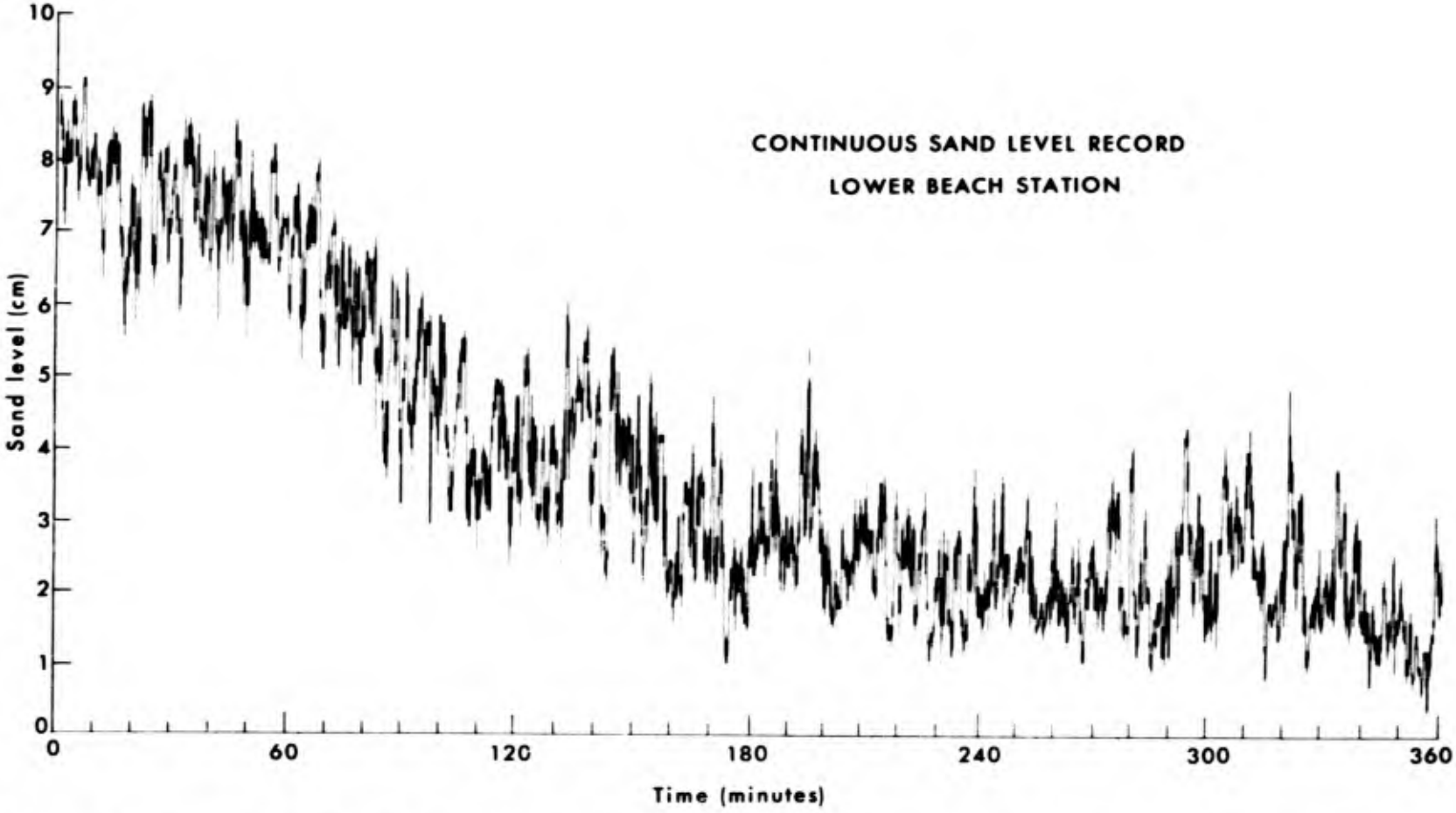

Figure 18a. Time series of sand level fluctuations at lower beach station. First 3 hours were erosional and latter 3 hours were approximately stable.

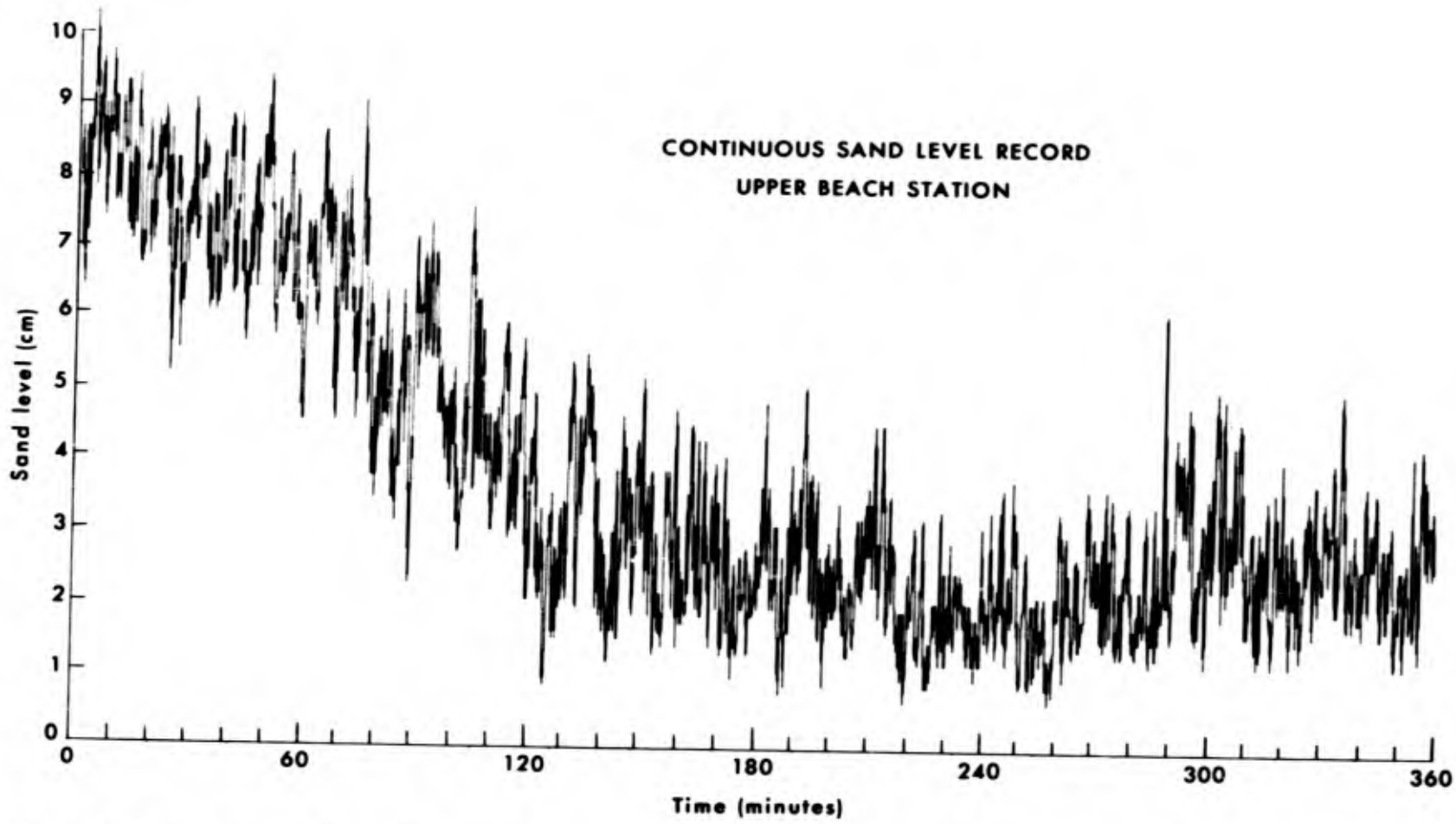

Figure 18b. Time series of sand level fluctuations at upper beach station. First 3 hours were erosional and latter 3 hours were approximately stable.

erosional episode and (2) rapid fluctuations. The trend, during the first 3 hours, was associated with a net profile retreat which was caused by a general increase in the breaker heights reaching the shoreline. The cessation of this trend at time, t, = 3 hours marked a rather definite transition from erosion to nonerosion.

Rapid fluctuations were isolated by removal of the trend from the original data and then analyzed using spectral analysis. The results of this analysis are shown in Figures 19a and b. These are separated on the basis of the times of erosion and nonerosion and on the basis of probe location. In all the spectra, more than 99 percent of the spectral power was concentrated in the frequencies less than 0.03 hertz.

It is generally known that a train of sand waves which develops in a stream possesses characteristic spectral features (Kennedy, 1969). Hino (1968) has shown, using dimensional considerations, that the frequency spectrum of sand waves should follow the -3 power law in the equilibrium subrange and the -2 power law at frequencies below the equilibrium subrange.

If the elevation of the sand surface from a given datum is given by η and the slope by $\eta' = d\eta/dx$, then the wave number power spectra is written

$$S_{nn}(k) = \frac{S_{n'n'}(k)}{(2\pi)^2 k^2} \tag{31}$$

where S denotes the power spectrum and k is the wave number $(2\pi/L)$. The angle of repose of the sand, ϕ, places a limit on the slope spectrum which in turn defines an equilibrium subrange dependent on ϕ and k. Dimensionally, in this subrange,

$$S_{n'n'}(k) = (2\pi)^2 f(\phi)\, k^{-1} \tag{32}$$

or

$$S_{nn}(k) = f(\phi)\, k^{-3} . \tag{33}$$

The wave number and frequency spectra are related by

$$P_{nn}(f) = S_{nn}(k) \frac{dk}{df} . \tag{34}$$

The terms f and k are related by $f = k\, c(k)$, in which c(k) is celerity. At lower wave numbers, where interaction between water and bed configuration becomes significant, celerity may be approximated by

$$c(k) = A\, k. \tag{35}$$

Combining Equations 31, 34, and 35 for ranges below the equilibrium subrange, the frequency spectrum is written as

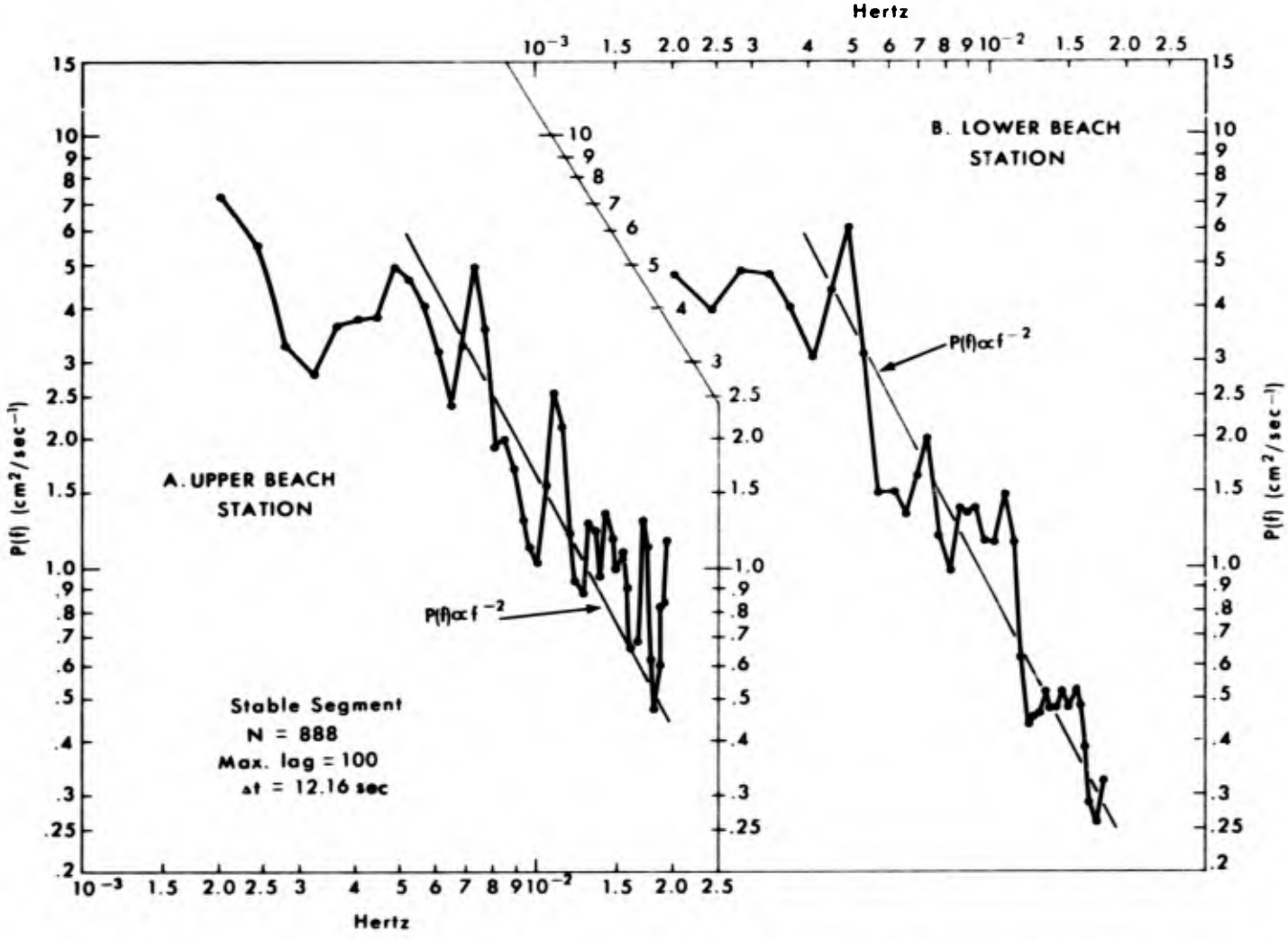

Figure 19a. Power spectra for sand level fluctuations during stable segment are plotted on log-log scale.

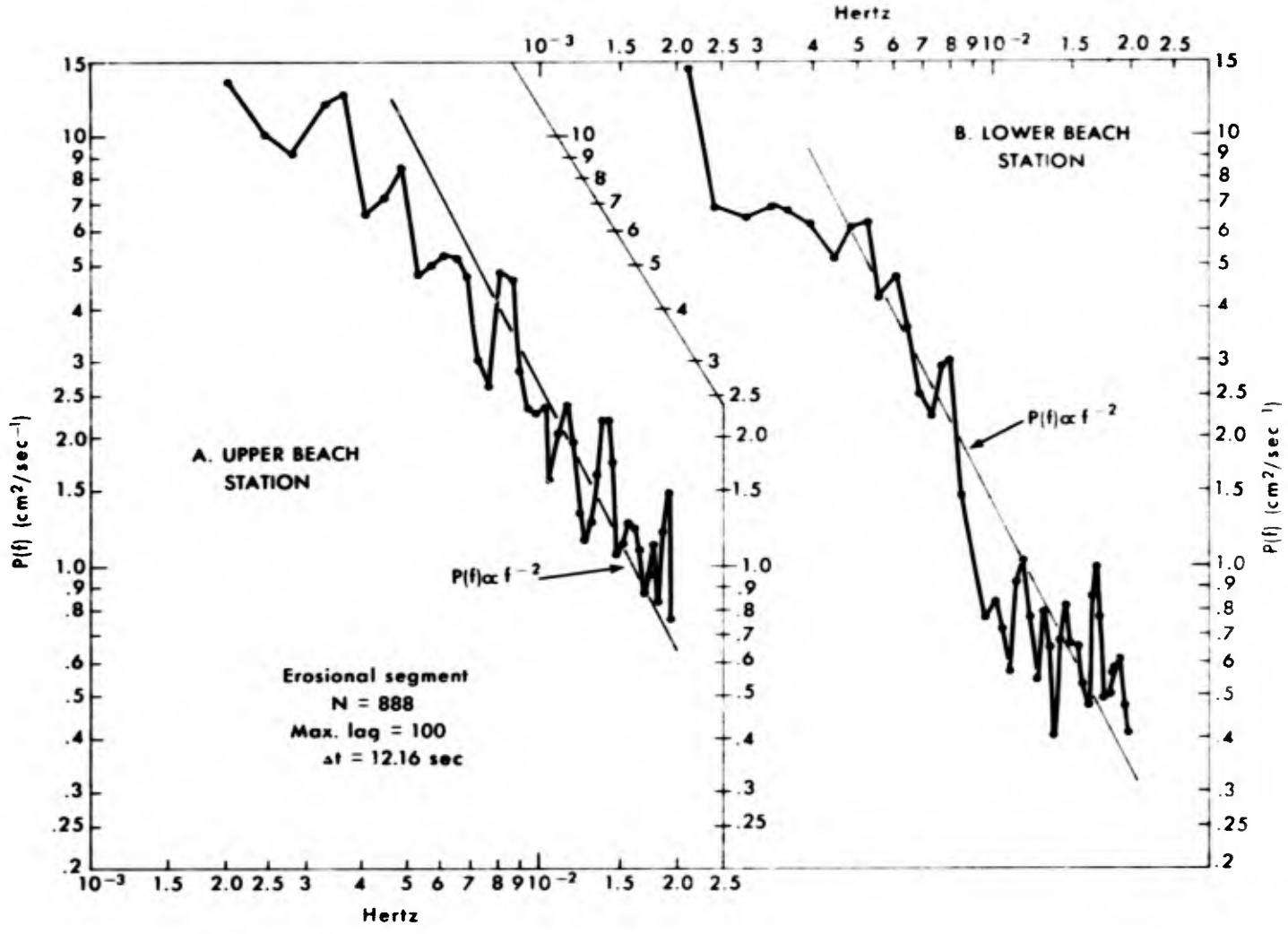

Figure 19b. Power spectra for sand level fluctuations during erosional segment are plotted on log-log scale.

$$P_{nn}(f) = \frac{f(\phi)\, A\, f^{-2}}{2} \qquad (36)$$

which shows the -2 power law dependence.

As shown in Figures 19a and b, these frequency spectra indicate a reasonable agreement with the -2 power law in both the erosional and nonerosional segments of the data. It should be noted that not only the -2 power dependence but also the general configuration of the spectra in this study are strikingly similar to those obtained by Ashida and Tanaka (1967), which were based on laboratory sand waves under undirectional flow. These agreements suggest that the observed sand level changes in this study involved a sand wave phenomenon. The presence of sand waves was not readily evident at the time of the field measurement, but this could have been the result of their lack of steepness.

The phase lag between the two beach stations was computed through a cross-spectral analysis for both the erosional and nonerosional segments of the data (Fig. 20). In both segments the lower station consistently lagged behind the upper beach station. This fact suggests that the sand waves moved from the upper beach to the lower beach, regardless of the net sand balance on the beach. Furthermore, a contrast in the behavior of sand waves between erosional and stable processes was noted. During the erosional process, the celerity of the sand wave exhibited a proportionality to frequency, as indicated in Figure 21. However, during the nonerosional process, the celerity failed to display any such dependence on frequencies over the range considered.

The data revealed no evidence of upslope migration of sand waves, suggesting that the material involved in the downslope migration of sand waves initially arrived on the upper beach as suspended load entrained in the uprush. The subsequent downslope movement of this material occurred as bedload in the backwash. Neither upslope nor downslope movement occurs in response to a single swash but results from many swashes over a period of several minutes.

CONCLUSION

It appears that the array of resistance and capacitance sensors used in this study is an effective means of investigating multiple interactions between input wave, swash, sand level, and ground water with sufficient resolution. However, for more complete control on interacting parameters, additional measurements of internal velocities in the swash using an array of current meters and of sediment movement using fluorescent tracer seem to be advisable.

The leading edge of the swash behaved similar to a unit mass with an initial momentum moving up an incline of constant slope against gravity. The initial swash momentum, calculated from the limiting potential energy of the input wave, resulted in underestimation by a factor of 3 to 4, suggesting that the kinetic, as well as the potential, energy of the input wave contributed to the formation of the initial swash momentum. In real processes, the initial swash momentum is further influenced by collision between successive swashes. Mathematical theories which assume breaking wave input cannot explain the collision process because they deal only with solitary input waves. Again, field measurements of actual swash momentum appear to be essential for future studies.

Collision between successive swashes at the lower beach is a phenomenon of fundamental importance, although it has not received sufficient attention in

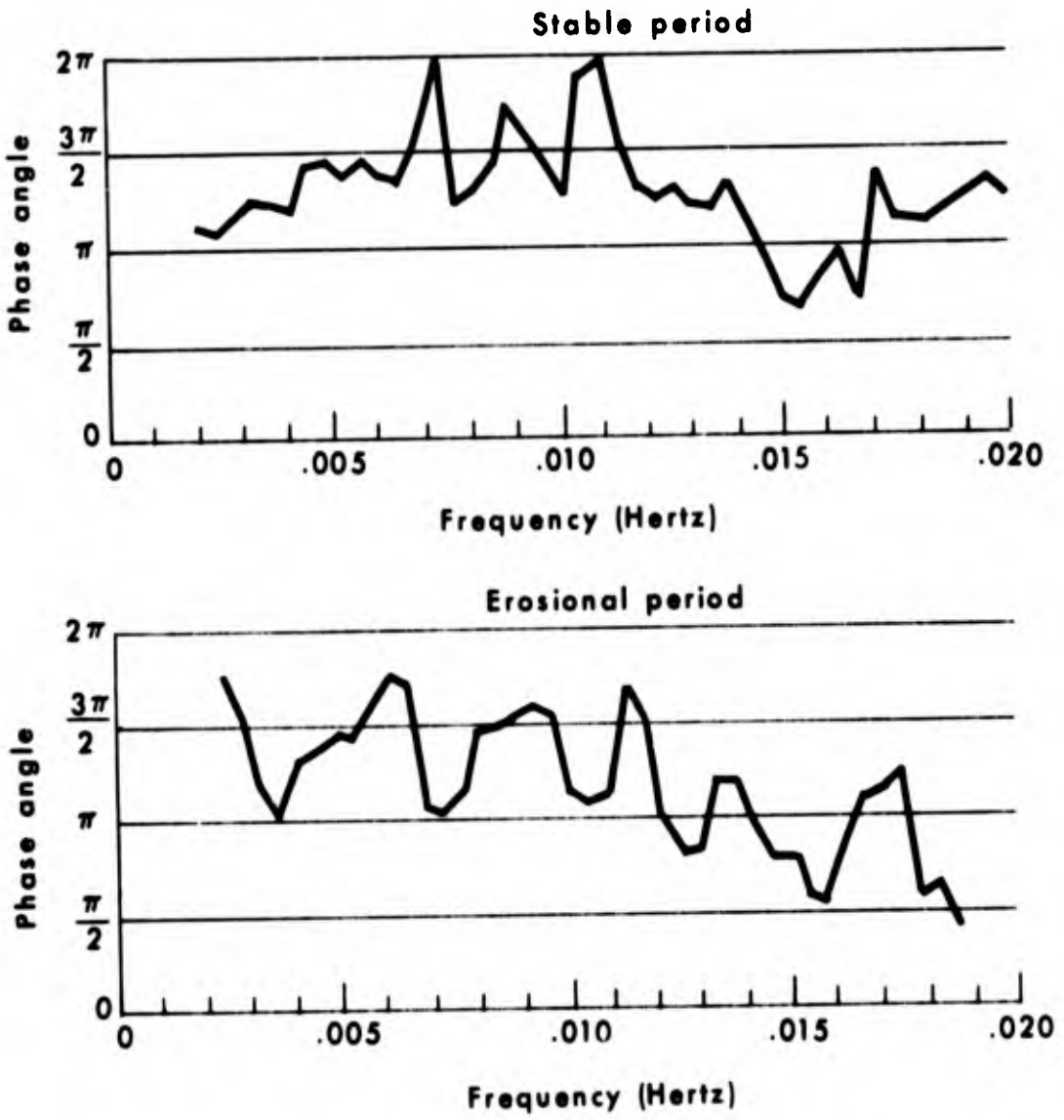

Figure 20. Phase angles between upper and lower beach stations for erosional and stable segments. The phase relation indicates that the upper beach consistently leads the lower beach in the applicable frequency band.

existing studies of both laboratory and theoretical approaches. Collision occurred because the inundation period at the base of the swash slope, which was controlled not only by the input wave characteristics but also by the beach slope, was consistently longer than the period of input waves. As a result, each input wave was unable to produce a full-cycle swash movement on the beach slope, and consequently the interswash period on the beach face was distinctly longer than the input wave period. Collision was intensified by increase in input wave energy reaching the shore, which in turn resulted in expansion of the band width under the interswash

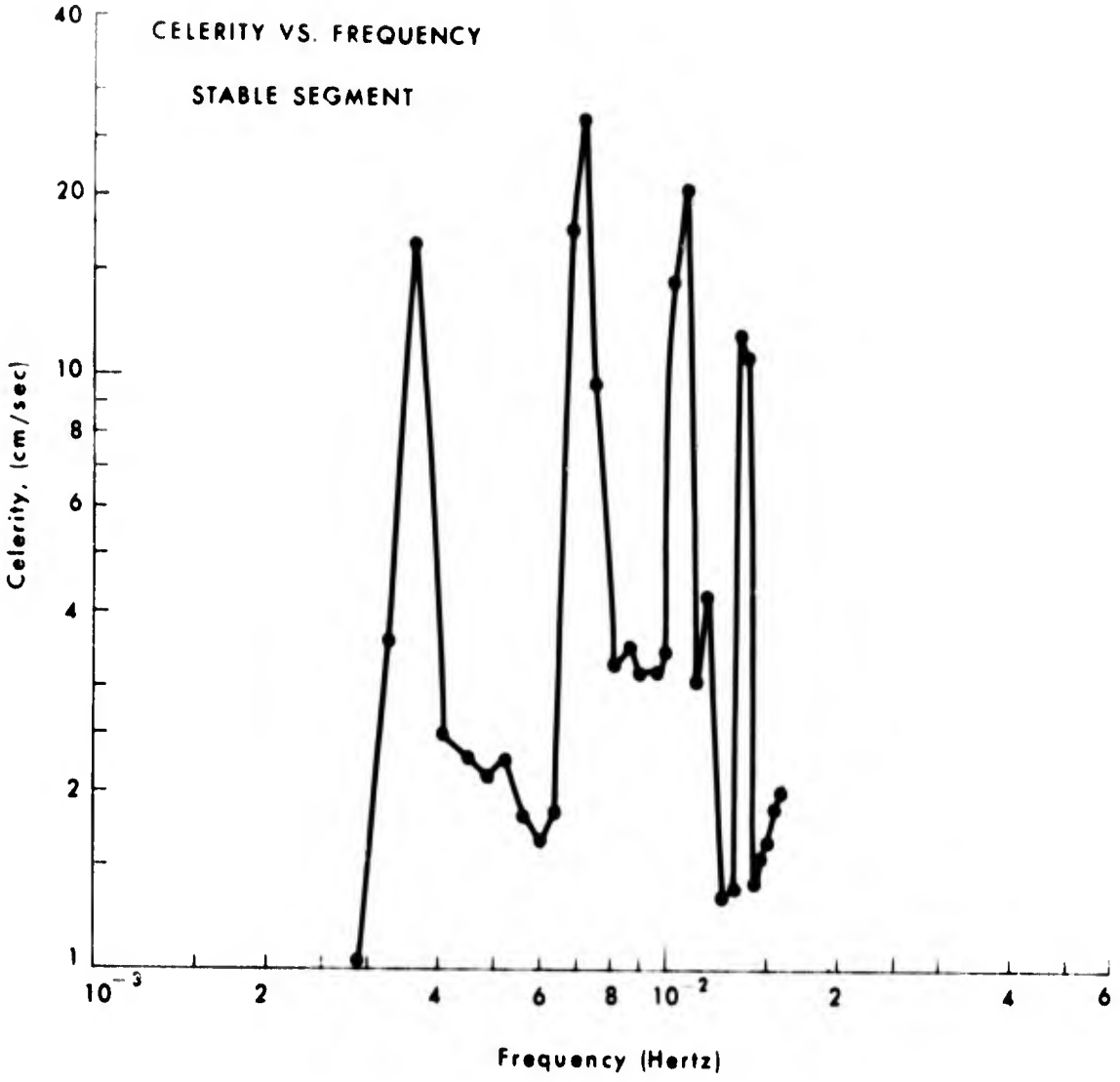

Figure 21a. Sand wave celerity during stable segment. Celerity is plotted only for frequencies which contained significant power concentrations.

spectral peak height. Concurrently, additional turbulence caused by the intensified collision caused the high-frequency swash spectral peak to increase in height.

The beach ground water responded sensitively to excitations over a broad range of gravity wave frequencies. Owing to the low-pass filtering properties of the beach matrix, beat excitations were transmitted most efficiently. The causative mechanism of the beat which was observed to persist at the base of the beach slope is not immediately clear, but it appears to be associated with a standing wave in the nearshore zone.

The sand level on the upper portion of the swash slope exhibited high-frequency fluctuations ($\sim 5 \times 10^{-3}$ hertz), and there were indications that they were related to a train of small-amplitude sand waves migrating downslope. It

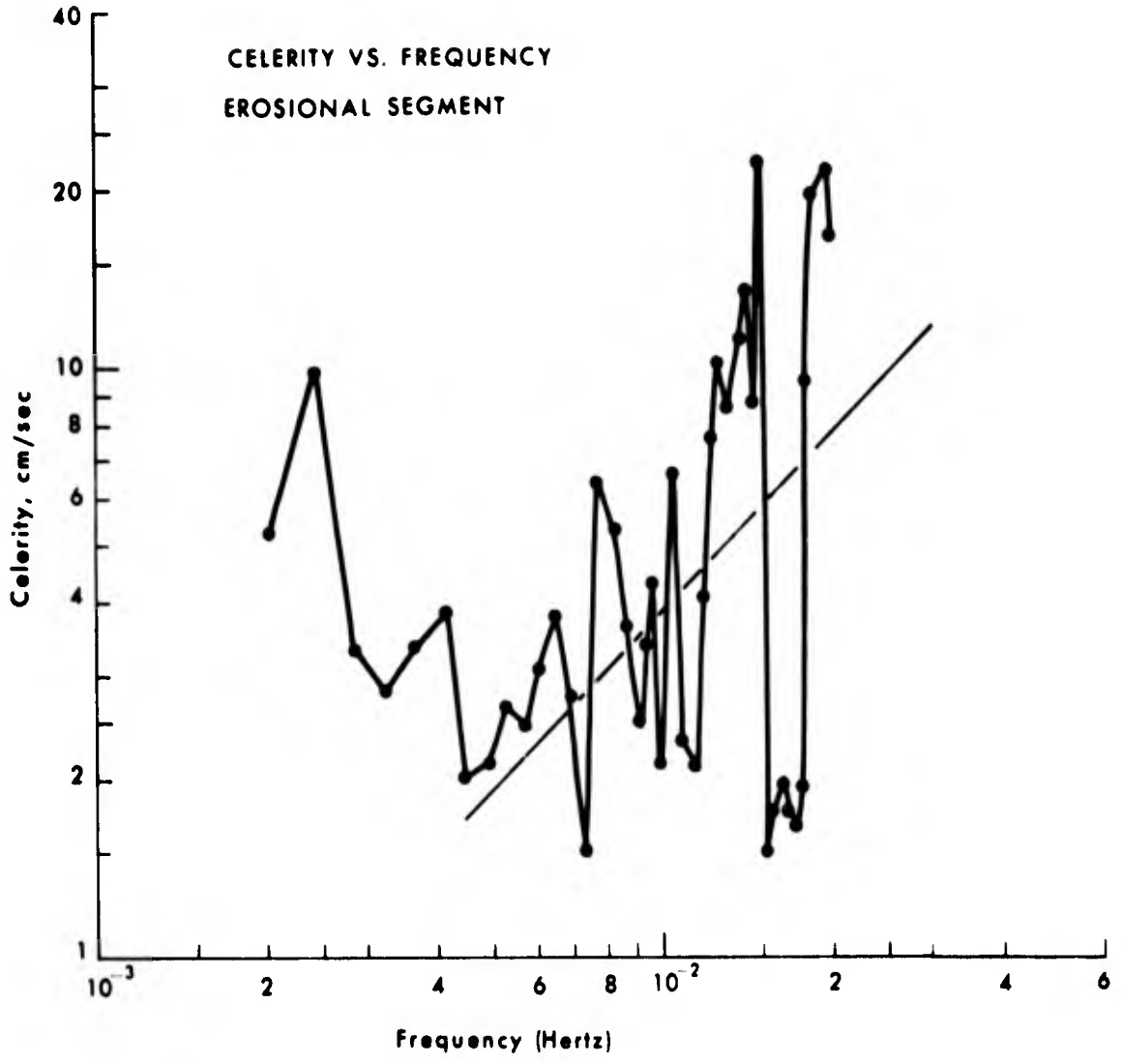

Figure 21b. Sand wave celerity during erosional segment. Celerity is plotted only for frequencies which contained significant power concentrations.

appeared that the beach material would move downslope dominantly as bedload in the form of sand waves and upslope as suspended load entrained in the uprush. In the absence of actual measurement of sediment movement, no definite relationship between sediment behavior and ground water could be established.

This study was limited to two-dimensional variability; the three-dimensional beach system should also be studied. There is the possibility that a longshore variability of the characteristics of both input swell reaching the shoreline and long-period standing waves could cause specific alongshore variability of swash characteristics and ground water fluctuations so as to produce such features as cusps and subaerial extension of a rhythmic topography.

REFERENCES

Ashida, K., and Y. Tanaka, 1967, A statistical study of sand waves. Proc., XII Congress Intern. Assoc. Hydraulic Res., pp. 103-110.

Battjes, J. A., 1971, Run-up distribution of breaking waves on slopes. J. Waterways, Harbors, and Coastal Engr. Div., Am. Soc. Civil Engrs., WW1, pp. 91-114.

Bendat, J. S., and A. G. Piersol, 1966, Measurement and analysis of random data. New York (John Wiley), 390 pp.

Biesel, F., 1951, Study of wave propagation in water at gradually varying depth. National Bureau of Standards, Circular 521, pp. 243-253.

Blackman, R. B., and J. W. Tukey, 1958, Measurement of power spectra. New York (Dover), 190 pp.

Collins, J. I., and W. Wier, 1969, Probabilities of wave characteristics in the surf zone. Tetra Tech Inc., Pasadena, Calif., Rept. No. TT-TC-149, 124 pp.

Dominick, T. F., B. Wilkins, and H. Roberts, 1971, Mathematical model for beach ground water fluctuations. Water Resources Res., 7(6):1626-1635.

Duncan, J. R., 1964, The effects of water table and tide cycle on swash-backwash sediment distribution and beach profile development. Marine Geol., 2:186-197.

Emery, K. O., and J. F. Foster, 1948, Water tables in marine beaches. J. Marine Res., 7(3):644-654.

Emery, K. O., and J. F. Gale, 1951, Swash and swash marks. Trans. Am. Geophys. Union, 32(1):31-36.

Grant, U. S., 1948, Influence of water-table on beach aggradation and degradation. J. Marine Res., 7(3):655-660.

Granthem, K. N., 1953, Wave run-up on sloping structures. Trans. Am. Geophys. Union, 34:720-724.

Hall, J. V., and G. M. Watts, 1953, Laboratory investigation of the vertical rise of solitary waves on impermeable slopes. U.S. Army Corps of Engrs., Beach Erosion Board, Tech. Memo. 33:1-14.

Harrison, W., C. S. Fang, and S. N. Wang, 1971, Ground water flow in a sandy tidal beach, i. One-dimensional finite element analysis. Water Resources Res., 7(5):1313-1321.

Hasselman, K., W. H. Munk, and G. MacDonald, 1963, Bispectra in ocean waves. In (M. Rosenblatt, ed.) Time series analysis, Chapter 8, pp. 125-139, New York (Wiley).

Haubrich, R. A., 1965, Earth noise, 5 to 500 millicycles per second. J. Geophys. Res., 70(6):1415-1427.

Hino, M., 1968, Equilibrium range spectra of sand waves formed by flowing water. J. Fluid Mech. no. 134, part 3, pp. 565-573.

Hom-ma, M., and C. J. Sonu, 1962, Rhythmic pattern of longshore bars related with sediment characteristics. Proc., VIII Conf. Coastal Engr., pp. 248-278.

Hosoi, M., and H. Mitsui, 1963, Wave run-up on sea dikes located in the surf zone or on the shore. Coastal Engr. in Japan, 6:1-6.

Hudson, R. Y., 1959, Laboratory investigation of rubble-mount breakwaters. J. Waterways and Harbors Div., Am. Soc. Civil Engrs., 85(3):108-113.

Hunt, I. A., 1959, Design of seawalls and breakwaters. J. Waterways and Harbors Div., Am. Soc. Civil Engrs., 85:123-152.

Kaplan, K., 1955, Generalized laboratory study of tsunami run-up. U.S. Army Corps of Engrs., Beach Erosion Board, Tech. Memo. 60:1 30.

Kennedy, J. F., 1969, The formation of sediment ripples, dunes, and antidunes. Ann. Rev. Fluid Mech., 1:147-168.

Kisel, C. C., 1969, Time series analysis of hydrologic data. Advan. Hydrosci., 5:1-112.

LeMéhauté, B., 1963, On non-saturated breakers and the wave run-up. Proc., VIII Conf. Coastal Engr., Mexico City, Nov. 1962, pp. 77-92.

_____, R. C. Y. Koh, and Li-San Hwang, 1968, A synthesis on wave run-up. J. Waterways and Harbors Div., Am. Soc. Civil Engrs., 94:77-92.

Longuet-Higgins, M. S., and D. W. Parkin, 1962, Sea waves and beach cusps. Geographical J., 128(2):194-201.

Longuet-Higgins, M. S., and R. W. Stewart, 1962, Radiation stress and mass transport in gravity waves, with application to 'surf beats.' J. Fluid Mech., 13:481-504.

McGoldrick, L. F., 1969, A system for the generation and measurement of capillary waves. Univ. Chicago, Dept. Geophys. Res., Tech. Rept. No. 3.

Meyer, R. E., 1970, Note on wave run-up. J. Geophys. Res., 75(3):687-690.

Miller, R., 1968, Experimental determination of run-up of undular and fully developed bores. J. Geophys. Res., 73:4497-4510.

Munk, W. H., 1949, Surf beats. Trans. Am. Geophys. Union, 30(6):374-424.

Pollack, L. W., and W. D. Hummon, 1971, Cyclic changes in interstitial water content, atmospheric exposure, and temperature in a marine beach. Limnology and Oceanography, 16(3):522-535.

Savage, R., 1959, Laboratory data on wave run-up on roughened and permeable slopes. U.S. Army Corps of Engrs., Beach Erosion Board, Tech. Memo. 109:1-28.

Saville, T., Jr., 1957, Wave run-up on composite slopes. VI Conf. Coastal Engr., Chapter 41, pp. 691-699.

_____, 1963, An approximation on the wave run-up frequency distribution. Proc., VIII Conf. Coastal Engr., Mexico City, Nov. 1962, pp. 48-59.

Shen, M. C., and R. E. Meyer, 1962, Climb of a bore on a beach, Part 2, Nonuniform beach slope, and Part 3, Run-up. J. Fluid Mech., 16:108-125.

Sibul, O., and E. G. Tickner, 1956, Model study of overtopping of wind-generated waves on levees with slopes of 1:3 and 1:6. U.S. Army Corps of Engrs., Beach Erosion Board, Tech. Memo. 80:1-19.

Sonu, C. J., 1973, Three-dimensional beach changes. J. Geol., 81(1):42-64.

_____, and J. L. van Beek, 1971, Systematic beach changes on the Outer Banks, North Carolina. J. Geol., 79(4):416-425.

Stoker, J. J., 1947, Surface waves in water of variable depth. Quart. Appl. Math., 5:1-54.

Strahler, A., 1966, Tidal cycle of changes on an equilibrium beach, Sandy Hook, New Jersey. J. Geol., 74(3):247-268.

Suhayda, J., 1972, Experimental study of the shoaling transformation of waves on a sloping bottom. Unpublished Ph.D. dissertation, Scripps Inst. Oceanography, Univ. Calif., San Diego, 106 pp.

Truxillo, S., 1970, Development of a resistance-wire wave gauge for shallow-water-wave and water-level investigations. Louisiana State Univ., Coastal Studies Bull. 4, pp. 73-76.

Tucker, J. M., 1950, Surf beats: sea waves of 1 to 5 minute period. Proc. Roy. Soc. London, A, 202:565-573.

Van Dorn, W. G., 1967, Run-up recipe for periodic waves on uniformly sloping beaches. Proc., Tenth Conf. Coastal Engr., 1:554-572.

Wiegel, R. L., 1964, Oceanographical engineering. New York (Prentice Hall), 532 pp.